Master of Science

60 points

2024 Spring

Dynamical Exchange-correlation Field in Low-dimensional Model Systems

Jinxiang Xu

May 2024

Devision of Mathematical Physics

Department of Physics, Lund University

Supervisor: Ferdi Aryasetiawan

Co-supervisor: Zhen Zhao

LUND UNIVERSITY

Abstract

Recently, a new formalism for calculating the Green function of many-particle systems was introduced, in which the self-energy is replaced by a dynamical exchange-correlation potential. The dynamical exchange-correlation potential is an exact generalization of the Slater $X\alpha$ exchange potential proposed in 1951, which includes the effects of correlations. It may be regarded as the counterpart of the Kohn-Sham potential in ground-state density-functional theory, providing in principle access to one-particle excitation spectra measured in (inverse) photoemission experiments.

The exchange-correlation potential and its associated hole have been previously investigated for the homogeneous electron gas within the random-phase approximation using the so-called plasmon-pole approximation. In this thesis, as a benchmark the exchange-correlation potential and hole have been calculated within the full random-phase approximation without resort to the plasmon-pole approximation for both the three- and two-dimensional electron gas.

The dynamical exchange-correlation potential formalism has also been extended to the Hubbard model in the arbitrary dimension within the random-phase approximation. Particularly, the results it yields have been evaluated and compared to the exact one for the Hubbard dimer.

Contents

List of acronyms

HFA Hatree-Fock approximation

HEG Homogeneous electron gas

DFT Density functional theory

LDA Local density approximation

KS Kohn-Sham

dD d-dimensional

the RPA Random-phase approximation

1 Introduction

(This section has been completely rewritten) Quantum mechanics was born at the beginning of the last century, and followed by rapid development of a few decades. Nonetheless, if it is applied to real materials that involve many-body interaction, the enormous size of Hilbert space makes it an impossible challenge to implement exact diagonalization. Inspired by the development of quantum field theory, the quantum many-body theory was established to calculate the properties of many-body systems.

As a pivotal quantity in this theory, the one-particle Green function (time-ordered) at zero temperature is defined as

$$iG(\mathbf{r},\mathbf{r}';t,t') = T\left\langle \Phi\right| \hat{\psi}(\mathbf{r};t)\hat{\psi}^{\dagger}(\mathbf{r}';t')\left|\Phi\right\rangle . \tag{1.1}$$

It can be interpreted as the probability amplitude for a particle created at the spacetime point $(\mathbf{r}';t')$ annihilating at $(\mathbf{r};t)$ in the ground state $|\Phi\rangle$ of a system. It encapsulates crucial information about many-electron systems. By definition, the expectation value of any one-particle quantity can be expressed in terms of the one-particle Green function. By the Galitskii-Migdal total energy formula [1], one can calculate the total ground-state energy with the one-particle Green function. Furthermore, it contains the information about the excitation spectra observed in (inverse) photoemission experiments.

Traditionally, the Green function for a given Hamiltonian is determined by the self-energy operator, calculated through various methods. Among these, many-body perturbation theory, based on Feynman diagrams, and the path integral method, relying on quantum Monte Carlo techniques, are prominent. In particular, for a system with only Coulomb interaction, the equation of motion of the Green function can be expressed in terms of the self-energy:

$$\left(i\frac{\partial}{\partial t}-h(r)\right)G(r,r';t')-\int dr''dt''\Sigma(\mathbf{r},\mathbf{r}'';t-t'')G(r'',r';t'')=\delta(r-r')\delta(t), \tag{1.2}$$

where

$$h(r)=-\frac{1}{2}\nabla^{2}+V_{\mathrm{ext}}(r)+V_{\mathrm{H}}(r) \tag{1.3}$$

and V_{H} is the Hatree potential. The self-energy term, acting as a convolution on G, determines the Green function globally in space and time. In contrast, by introducing a dynamical exchange-correlation field [2], the self-energy term is replaced, yielding

$$\left(i\frac{\partial}{\partial t}-h(r)-V_{\mathrm{xc}}(r,r';t)\right)G(r,r';t)=\delta(r-r')\delta(t), \tag{1.4}$$

where the non-local convolution is replaced by the local field term. It provides a straightforwad interpretation for V_{xc} as an effective field felt by the quasiparticle.

In addition to a more straightforward description in space and time, the superiority of a local quantity rather than a non-local quantity in electronic structure was found in early 1950's. Introduced by Slater [3] to circumvent the difficulty caused by the orbital-dependence and nonlocal exchange operator in the computation of Hatree-Fock orbitals, Slater's exchange potential can also be interpreted as an effective field for the quasiparticle. Curiously, the quasiparticle dispersion of the homogeneous electron gas (HEG) calculated using the Slater exchange potential is much closer to the correct result, in contrast to the Hatree-Fock result, which doubles the occupied band width. As a generalization of Slater's exchange hole, the dynamical exchange-correlation hole is expected to do a better job at some aspects.

The typical self energy expressed in terms of Feynman diagrams looks like:

$\Sigma(k) =$ 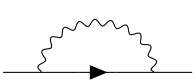 $+$ 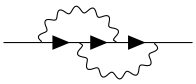 $+ \ldots$ (1.5)

The spirit of perturbation indicates the accuracy of results should be improved by including more diagrams. However, it is not always the case and the selection of diagrams is indeed tricky. For instance, to approximate the occupied band width of the HEG, if one chooses to calculate the self-energy within the GW approximation, then there is a subtlety needed to be considered. By setting $t' = 0$, the GW self-energy is given by

$$\Sigma^{GW}(r, r'; t) = iG(r, r'; t)W(r', r; t), \tag{1.6}$$

where $W(r, r'; t)$ is the screened Coulomb potential. Regarding the choice of the Green function, if one performs the Dyson equation iteratively until the self-consistency is reached, which is called the self-consistent GW approximation, it turns out the corresponding band width is broadened relative to the free band width. Nonetheless, by directly using the noninteracting Green function, which is known as one-shot GW approximation, the correct band narrowing is surprisingly reproduced.

Due to all of these complexity in the self-energy formalism, we hope to find a relatively simple and straightforward way as density functional theory (DFT) to obtain the Green function. Fortunately, there is one property of dynamical exchange-correlation hole

$$\rho_{\mathrm{xc}}(r, r', r'' = r; t) = -\rho(r), \tag{1.7}$$

which relates it with the ground state density. This fact provides the possibility to develop a local density approximation (LDA) as in DFT. If it is feasible, instead of performing the complicated calculation of Feynman diagrams, one can construct V_{xc} by tuning a few parameters. One may argue that this could work with self-energy as well. However, the self-energy is not easy to be parameterized in terms of the density because of its non-local nature, which is against our desire for a simple theory.

The key point in DFT is to approximate the exchange-correlation energy E_{xc} defined in

Kohn-Sham (KS) orbital equation:

$$-\frac{1}{2}\nabla^2\psi_i + v_{\mathrm{KS}}\psi_i = \varepsilon_i\psi_i, \tag{1.8}$$

where v_{KS} is given by

$$v_{\mathrm{KS}} = v_{\mathrm{ext}} + v_{\mathrm{H}} + \frac{\delta E_{\mathrm{xc}}}{\delta\rho}. \tag{1.9}$$

Analogously, the current direction of dynamical exchange-correlation field formalism involves finding proper approximations for the exchange-correlation potential in various model systems. Recent investigations have applied this approach to the 3-dimensional (3D) HEG [6], the 1D Hubbard chain [7] as well as the 1D anti-ferromagnetic Heisenberg spin chain [8]. The HEG has served as a simple model to mimic the behavior of valence electrons for quite a long time. The effects of exchange and correlations in the presence of Coulomb interaction have been studied thoroughly by using the self-energy formalism and some other conventional methods. Some prominent features could be accounted for by the exchange and correlation hole and potential within the random-phase approximation (RPA) as well, which demonstrates the correctness of this new formalism[6]. The Hubbard model, despite the simple appearance of Hamiltonian, can provide insight into systems containing the localized $3d$ transition metals and the $4f$ lanthanides.

Recognizing the unique properties in low-dimensional systems, this thesis concentrates on the 2D HEG and Hubbard dimer embedded in the 2D plane. The dynamical exchange-correlation hole and potential are investigated in the 2D HEG within the RPA to gain insights into its unique physics. This formalism is also applied to the Hubbard dimer and compared with the exact results [7] to evaluate the quality of the RPA. Additionally, the correlation hole and potential of the 3D electron gas, which has been investigated previously within the plasmon-pole approximation [6], is calculated with the full RPA.

Unfortunately, due to time constraints, the correlation hole and potential for the 2D electron gas are only computed in an approximate manner using an interpolation scheme and as a consequence might lose some subtle details. Even so, it displays some important features as expected.

2 Theory

2.1 General formula for the exchange-correlation hole

In the exchange-correlation potential formalism the equation of motion of the equilibrium zero-temperature time-ordered Green function is given by[2]

$$\left(i\frac{\partial}{\partial t} - h(r) - V_{\rm xc}(r,r';t)\right) G(r,r';t) = \delta(r-r')\delta(t), \tag{2.1}$$

where

$$h(r) = -\frac{1}{2}\nabla^2 + V_{\rm ext}(r) + V_{\rm H}(r), \tag{2.2}$$

in which $V_{\rm ext}$ and $V_{\rm H}$ are the external field and the Hartree potential, respectively, and $r = (\mathbf{r}, \sigma)$ labels both space and spin variables.

The exchange-correlation potential $V_{\rm xc}$ is the Coulomb potential of the exchange-correlation hole $\rho_{\rm xc}$:

$$V_{\rm xc}(r,r';t) = \int dr'' v(r-r'')\rho_{\rm xc}(r,r',r'';t). \tag{2.3}$$

The instantaneous nature of Coulomb interaction implies that $t = t''$. The exchange-correlation hole fulfills a sum rule [2]

$$\int d^3r''\rho_{\rm xc}(r,r',r'';t) = -\delta_{\sigma\sigma''}\theta(-t), \tag{2.4}$$

which is the generalization of the static case. Note that for the electron ($t > 0$) the right-hand side is always zero, which reflects a fundamental difference between the hole and electron. Another unique property is that the density fulfills the following exact condition,

$$\rho_{\rm xc}(r,r',r''=r;t) = -\rho(r), \tag{2.5}$$

for *any* r, r', and t. One can verify by using Schwinger functional technique the following formula [6]:

$$\rho_{\rm xc}(1,2,3) = i\frac{\delta}{\delta\phi(3)}\ln G(1,2), \tag{2.6}$$

where ϕ is a probing field, which is set to zero at the end, and $1 = (r_1, t_1)$, etc., with $t_1 = t_3$.

For the practical use, this equation can be simplified to [6]

$$\begin{aligned}\rho_{xc}(1,2,3)G(1,2) =& i\int d4G(1,4)\left\{\delta(3-4) + \frac{\delta V_{\rm H}(4)}{\delta\phi(3)}\right\}G(4,2) \\ &+ i\int d4d5G(1,4)\frac{\delta\Sigma(4,5)}{\delta\phi(3)}G(5,2),\end{aligned} \tag{2.7}$$

where Σ is the self-energy. In some cases, it is preferable to investigate these concepts in a set of base orbitals $\{\varphi_i\}$:

$$i\frac{\partial}{\partial t}G_{ij}(t) - \sum_k h_{ik}G_{kj}(t) - \sum_{kl} V^{\mathrm{xc}}_{ik,lj}(t)G_{kl}(t) = \delta_{ij}\delta(t), \tag{2.8}$$

where G_{ij} and h_{ik} are the matrix elements of G and h in the orbitals and

$$V^{\mathrm{xc}}_{ik,lj}(t) = \int d^3r d^3r' \varphi^*_i(r)\varphi_k(r)V_{\mathrm{xc}}(r,r';t)\varphi^*_l(r')\varphi_j(r'). \tag{2.9}$$

In practice, there exists a formal solution by solving the following Dyson-like equation self-consistently:

$$G(r,r';t) = G^{\mathrm{H}}(r,r';t) + \int dr''dt' G^{\mathrm{H}}(r,r'';t-t')V_{\mathrm{xc}}(r'',r';t')G(r'',r';t'). \tag{2.10}$$

Taking the Kohn-Sham DFT as a point of reference, one may choose the Kohn-Sham Green function G^{KS} as a starting point, in which case V_{xc} should be replaced by $V_{\mathrm{xc}} - V^{\mathrm{KS}}_{\mathrm{xc}}$. In contrast to the Hartree Green function, the Kohn-Sham Green function is closer to the true one since it gives the ground-state density. Utilising this property yields the following relation [2]:

$$\lim_{r'\to r;t\to 0^-}\left(-i\frac{\partial}{\partial t} - \frac{\nabla^2}{2}\right)[G(r,r';t) - G^{\mathrm{KS}}(r,r';t)] = -i[V_{\mathrm{xc}}(r,r';0^-) - V^{\mathrm{KS}}_{\mathrm{xc}}(r)]\rho(r). \tag{2.11}$$

Due to the static nature of $V^{\mathrm{KS}}_{\mathrm{xc}}$, this relation is non-trivial in general. Because Eq. (2.10) involves integral, it is preferable to go to the space spanned by discrete eigen-basis (normally momentum space for translationally symmetric system), where the spectrum becomes [7]

$$G_{ij}(t) = G^{\mathrm{H}}_{ij}(t) + \sum_k \int dt' G^{\mathrm{H}}_{ik}(t-t')F_{kj}(t'), \tag{2.12}$$

in which

$$F_{kj}(t') = \sum_{lm} V^{\mathrm{xc}}_{kl,mj}(t')G_{lm}(t'). \tag{2.13}$$

This quantity is important and will appear quite often, which makes the iterative solution very useful.

2.2 the RPA in the exchange-correlation potential formalism

Within the RPA, after neglecting the vertex correction, replacing $r_1 \to r$, $r_2 \to r'$, and $r_3 \to r''$ and taking into account the fact that $t_1 = t_3 = t$ and $t_2 = 0$, the equation determining the exchange-correlation hole takes the form that is first introduced in [6], namely

$$\begin{aligned}\rho_{xc}(r,\ r',\ r'';t)G(r,\ r';t) = iG(r,\ r'';0^-)G(r'',\ r';t)\\ +i\int dr_4dt_4G(r,\ r_4;t-t_4)K(r_4,\ r'';t_4-t)G(r_4,\ r';t_4),\end{aligned} \tag{2.14}$$

which is used most often in the thesis. The first term on the right-hand side corresponds to the exchange hole whereas the second term corresponds to the correlation hole. The exchange hole itself fulfills Eq. (2.4) and Eq. (2.5). In Eq 2.14, we have defined

$$\begin{aligned}K(r_4,\ r'';t_4-t) \equiv&\frac{\delta V_{\rm H}(r_4;t_4)}{\delta\phi(r'';t)}\\ =&\int dr_5 v(r_4-r_5)\chi(r_5,r'';t_4-t),\end{aligned} \tag{2.15}$$

where

$$\chi(r_5,r'';t_4-t) = \frac{\delta\rho(r_5,t_4)}{\delta\phi(r'';t)} \tag{2.16}$$

is known as the linear density response function. It can be expanded in powers of the polarization P as a Dyson-like equation,

$$\begin{aligned}\chi(r_5,r'';t_4-t) =&P(r_5,r'';t_4-t)\\ &+\int dr_6dt_6P(r_5,r_6;t_4-t-t_6)v(r_6-r'')P(r_6,r'';t_6)+\ldots\end{aligned} \tag{2.17}$$

which can be cast into a more compact form in frequency-momentum space:

$$\chi(\mathbf{q},\omega) = \frac{P(\mathbf{q},\omega)}{1-P(\mathbf{q},\omega)v(q)}. \tag{2.18}$$

This well-established formula will be frequently used to determine the correlation potential. In the traditional diagrammatic approach, the noninteracting Green function is used in the calculation. Despite of its simplicity, this prescription amazingly agrees with the experimental result better than using a renormalized Green function. In the exchange-correlation potential formalism, one can argue that the use of a noninteracting Green function is better by evaluating the integral in Eq. (2.4). With a noninteracting Green function, due to the orthogonality of orbital functions, it is easy to verify that the exchange hole itself fulfill

the sum rule, and the correlation hole actually does not contribute because the density fluctuations due to the polarization integrate to zero [6],

$$\int dr'' \rho_{\mathrm{x}}(r, r', r''; t < 0) = -1.$$
$$\int dr'' \rho_{\mathrm{c}}(r, r', r''; t) = \int dr'' \rho_{\mathrm{x}}(r, r', r''; t > 0) = 0. \tag{2.19}$$

In contrast, there is no obvious reason that it is the case for the renormalized Green function.

Although there is in principle a proper self-energy such that all the terms together in the right-hand side of Eq. (2.7) fulfill the sum rule, it is apparently much simpler to work with a noninteracting Green function than with a renormalized one. Therefore, one would desire to investigate the consequences of using a noninteracting Green function. The proper vertex correction has been presented in [6].

In the RPA with a noninteracting Green function, the polarization is given by

$$P^0(r, r'; t) = -iG^0(r, r'; t)G^0(r', r; -t), \tag{2.20}$$

and its Fourier transformation with respect to time is given by

$$P^0(r, r'; \omega) = -i \int \frac{d\omega'}{2\pi} G^0(r, r'; \omega + \omega')G^0(r', r; \omega'), \tag{2.21}$$

$$= \sum_{\mathbf{k}n}^{\mathrm{occ}} \sum_{\mathbf{k}'n'}^{\mathrm{unocc}} \left\{ \frac{\varphi^*_{\mathbf{k}n}(r)\varphi_{\mathbf{k}'n'}(r)\varphi^*_{\mathbf{k}'n'}(r')\varphi_{\mathbf{k}n}(r')}{\omega - \varepsilon_{\mathbf{k}'n'} + \varepsilon_{\mathbf{k}n} + i\delta} \right.$$
$$\left. - \frac{\varphi_{\mathbf{k}n}(r)\varphi^*_{\mathbf{k}'n'}(r)\varphi_{\mathbf{k}'n'}(r')\varphi^*_{\mathbf{k}n}(r')}{\omega + \varepsilon_{\mathbf{k}'n'} - \varepsilon_{\mathbf{k}n} - i\delta} \right\}. \tag{2.22}$$

where $\varphi_{\mathbf{k}n}$ is the eigenfunction of noninteracting Hamiltonian characterized by $\mathbf{k}$ and n. It can be seen P^0 obeys the following symmetry

$$P^0(r, r'; -\omega) = P^0(r, r'; \omega),$$
$$P^0(r, r'; \omega) = P^0(r', r; \omega), \tag{2.23}$$

valid for systems with time-reversal symmetry. Since we focus on the stationary systems in the absence of magnetic field, Eq. (2.23) is certainly valid in our cases.

2.3 The d-dimensional homogeneous electron gas in the RPA

In this thesis, the noninteracting Green function of the HEG is always used within the RPA. If considering a d-D cubic box, then it is given by

$$\begin{aligned} iG_0(r,r';t) =& \frac{1}{L^d}\sum_{k>k_\mathrm{F}} e^{i\mathbf{k}\cdot(\mathbf{r}-\mathbf{r}')}e^{-i\varepsilon_k t}\theta(t) \\ & - \frac{1}{L^d}\sum_{k\le k_\mathrm{F}} e^{i\mathbf{k}\cdot(\mathbf{r}-\mathbf{r}')}e^{-i\varepsilon_k t}\theta(-t), \end{aligned} \tag{2.24}$$

where $\epsilon_k = \frac{1}{2}k^2$, k_F is the magnitude of Fermi wave vector (or Fermi level), and L is the length of the box. It is understood that $\sigma = \sigma'$. For the HEG, $\mathbf{r}$ could be chosen as the origin, i.e., $\mathbf{r} = 0$, and one can define the new variables $\mathbf{R} = \mathbf{r}' - \mathbf{r}$, $\mathbf{R}' = \mathbf{r}'' - \mathbf{r}$ and $\mathbf{R}'' = \mathbf{r}'' - \mathbf{r}'$ to facilitate the derivation as in Figure 1.

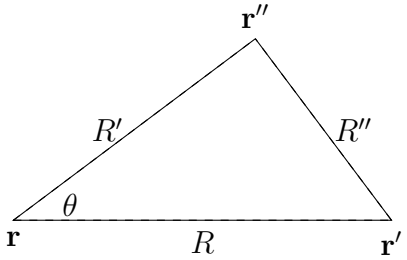

Figure 1: Definition of the radial variables R, R' and R''. They are related to the angle θ by $R''^2 = R^2 + R'^2 - 2RR'\cos\theta$

The exchange hole ($t < 0$) is given by

$$\begin{aligned} &\rho_\mathrm{x}(R,R',R'';t<0)\sum_{k\le k_\mathrm{F}} e^{-i\mathbf{k}\cdot\mathbf{R}}e^{-i\varepsilon_k t} \\ &= -\frac{1}{L^d}\sum_{k'\le k_\mathrm{F}} e^{-i\mathbf{k}'\cdot\mathbf{R}'} \times \sum_{k\le k_\mathrm{F}} e^{i\mathbf{k}\cdot\mathbf{R}''}e^{-i\varepsilon_k t}. \end{aligned} \tag{2.25}$$

For the exchange particle ($t > 0$), it is

$$\begin{aligned} &\rho_\mathrm{x}(R,R',R'';t>0)\sum_{k>k_\mathrm{F}} e^{-i\mathbf{k}\cdot\mathbf{R}}e^{-i\varepsilon_k t} \\ &= -\frac{1}{L^d}\sum_{k'\le k_\mathrm{F}} e^{-i\mathbf{k}'\cdot\mathbf{R}'} \times \sum_{k>k_\mathrm{F}} e^{i\mathbf{k}\cdot\mathbf{R}''}e^{-i\varepsilon_k t}. \end{aligned} \tag{2.26}$$

By the four-dimensional inverse Fourier transformation

$$K(r_4,r'';t_4-t) = \frac{1}{\Omega}\sum_q \int \frac{d\omega}{2\pi} e^{-i\mathbf{q}\cdot(\mathbf{r}_4-\mathbf{r}'')}e^{-i\omega(t_4-t)}K(q,\omega), \tag{2.27}$$

and Eq. (2.18), the correlation hole can be calculated in terms of $P(q,\omega)$. Note there is only magnitude dependence on the momentum for these quantities due to the isotropy in the HEG. The correlation hole ($t<0$) is given by [6]

$$\rho_{\rm c}(R,R',R'';t<0)\sum_{k\leq k_{\rm F}} e^{-i\mathbf{k}\cdot\mathbf{R}}e^{-i\varepsilon_k t} = -(A_1+A_2), \tag{2.28}$$

where

$$\begin{aligned} A_1 =& \frac{1}{L^d}\sum_{k\leq k_{\rm F}} e^{-i\mathbf{k}\cdot\mathbf{R}'}\sum_{k'>k_{\rm F}} e^{i\mathbf{k}'\cdot\mathbf{R}''} \\ &\times\int\frac{d\omega}{2\pi}\,K(|\mathbf{k}'-\mathbf{k}|,\,\omega)\frac{e^{i(\omega-\varepsilon_k)t}}{\omega-\varepsilon_k+\varepsilon_{k'}-i\eta}. \end{aligned} \tag{2.29}$$

$$\begin{aligned} A_2 =& -\frac{1}{L^d}\sum_{k>k_{\rm F}} e^{-i\mathbf{k}\cdot\mathbf{R}'}\sum_{k'\leq k_{\rm F}} e^{i\mathbf{k}'\cdot\mathbf{R}''} \\ &\times\int\frac{d\omega}{2\pi}\,K(|\mathbf{k}'-\mathbf{k}|,\,\omega)\frac{e^{-i\varepsilon_{k'}t}}{\omega-\varepsilon_k+\varepsilon_{k'}+i\eta}. \end{aligned} \tag{2.30}$$

For the correlation particle ($t>0$), it is

$$\rho_{\rm c}(R,R',R'';t>0)\sum_{k>k_{\rm F}} e^{-i\mathbf{k}\cdot\mathbf{R}}e^{-i\varepsilon_k t} = B_1+B_2, \tag{2.31}$$

where

$$\begin{aligned} B_1 =& \frac{1}{L^d}\sum_{k\leq k_{\rm F}} e^{-i\mathbf{k}\cdot\mathbf{R}'}\sum_{k'>k_{\rm F}} e^{i\mathbf{k}'\cdot\mathbf{R}''} \\ &\times\int\frac{d\omega}{2\pi}\,K(|\mathbf{k}'-\mathbf{k}|,\,\omega)\frac{e^{-i\varepsilon_{k'}t}}{\omega-\varepsilon_k+\varepsilon_{k'}-i\eta}. \end{aligned} \tag{2.32}$$

$$\begin{aligned} B_2 =& -\frac{1}{L^d}\sum_{k>k_{\rm F}} e^{-i\mathbf{k}\cdot\mathbf{R}'}\sum_{k'\leq k_{\rm F}} e^{i\mathbf{k}'\cdot\mathbf{R}''} \\ &\times\int\frac{d\omega}{2\pi}\,K(|\mathbf{k}'-\mathbf{k}|,\,\omega)\frac{e^{i(\omega-\varepsilon_k)t}}{\omega-\varepsilon_k+\varepsilon_{k'}+i\eta}. \end{aligned} \tag{2.33}$$

To calculate the integral over ω one utilizes the spectral representation of $K(q,\omega)$:

$$K(q,\omega) = \int_{-\infty}^{0} d\omega'\,\frac{L(q,\omega')}{\omega-\omega'-i\delta} + \int_{0}^{\infty} d\omega'\,\frac{L(q,\omega')}{\omega-\omega'+i\delta}, \tag{2.34}$$

where

$$L(q,\omega) = -\frac{1}{\pi}\mathrm{sign}(\omega)\mathrm{Im}K(q,\omega). \tag{2.35}$$

By using the property

$$L(k,-\omega) = -L(k,\omega) \tag{2.36}$$

specifying that the coutour integral in the complex ω plane is closed in the lower-half plane, for $t<0$, one obtains

$$\begin{aligned} A_1 =& \frac{1}{L^d}\sum_{k\le k_\mathrm{F}} e^{-ik\cdot\mathbf{R}'}e^{-i\varepsilon_k t}\sum_{k'>k_\mathrm{F}} e^{i\mathbf{k}'\cdot\mathbf{R}''} \\ & \times M(|\mathbf{k}'-\mathbf{k}|,\varepsilon_{k'}-\varepsilon_k;t); \end{aligned} \tag{2.37}$$

$$\begin{aligned} A_2 =& \frac{1}{L^d}\sum_{k>k_\mathrm{F}} e^{-ik\cdot\mathbf{R}'}\sum_{k'\le k_\mathrm{F}} e^{i\mathbf{k}'\cdot\mathbf{R}''}e^{-i\varepsilon_{k'}t} \\ & \times M(|\mathbf{k}'-\mathbf{k}|,\varepsilon_k-\varepsilon_{k'},0); \end{aligned} \tag{2.38}$$

$$\begin{aligned} B_1 =& \frac{1}{L^d}\sum_{k\le k_\mathrm{F}} e^{-ik\cdot\mathbf{R}'}\sum_{k'>k_\mathrm{F}} e^{i\mathbf{k}'\cdot\mathbf{R}''}e^{-i\varepsilon_{k'}t} \\ & \times M(|\mathbf{k}'-\mathbf{k}|,\varepsilon_{k'}-\varepsilon_k,0); \end{aligned} \tag{2.39}$$

$$\begin{aligned} B_2 =& \frac{1}{L^d}\sum_{k>k_\mathrm{F}} e^{-ik\cdot\mathbf{R}'}e^{-i\varepsilon_k t}\sum_{k'\le k_\mathrm{F}} e^{i\mathbf{k}'\cdot\mathbf{R}''} \\ & \times M(|\mathbf{k}'-\mathbf{k}|,\varepsilon_k-\varepsilon_{k'},-t), \end{aligned} \tag{2.40}$$

where

$$M(q,\omega;t) = \int_0^\infty d\omega' L(q,\omega')\frac{-ie^{i\omega' t}}{\omega'+\omega}. \tag{2.41}$$

In the thermodynamic limit, i.e. $L\to\infty$, the summation over the discrete value of $\mathbf{k}$ in dD momentum space should be rewritten as

$$\sum_{\mathbf{k}} \Rightarrow \left(\frac{L}{2\pi}\right)^d \int_{\mathbf{k}} \tag{2.42}$$

In this case, Eq. (2.24) becomes

$$\begin{aligned} iG_0(r,r;t) =& \frac{1}{(2\pi)^d}\int_{k_\mathrm{F}}^\infty dk\, k^{(d-1)}\int d\mathbf{\Omega}_{d-1}\, e^{-i\mathbf{k}\cdot\mathbf{R}}e^{-i\varepsilon_k t}\theta(t) \\ & - \frac{1}{(2\pi)^d}\int_0^{k_\mathrm{F}} dk\, k^{(d-1)}\int d\mathbf{\Omega}_{d-1}\, e^{-i\mathbf{k}\cdot\mathbf{R}}e^{-i\varepsilon_k t}\theta(-t), \end{aligned} \tag{2.43}$$

where $\mathbf{\Omega}_{d-1}$ is the element of solid angle on the $(d-1)$-dimensional sphere surface. It is always unsolvable analitically, and numerical tools need to be used to solve it. In this thesis, $d = 2,\ 3$ is the focus.

As the quantity that is the potential after being integrated over the radial separation, the spherical-averaged density reveals interesting physics itself. To calculate it, taking the spherical-averaged exchange hole density as an example, after integrating Eq. (2.25) over the solid angle, it is given by

$$\bar{\rho}_{\mathrm{x}}(R, R', R''; t < 0) = \int d\mathbf{\Omega}_{d-1} \frac{-\frac{1}{L^d} \sum_{k' \leq k_{\mathrm{F}}} e^{-i\mathbf{k}'\cdot\mathbf{R}'} \times \sum_{k \leq k_{\mathrm{F}}} e^{i\mathbf{k}\cdot\mathbf{R}''} e^{-i\varepsilon_k t}}{\sum_{k \leq k_{\mathrm{F}}} e^{-i\mathbf{k}\cdot\mathbf{R}} e^{-i\varepsilon_k t}}. \tag{2.44}$$

It could be interesting to compare the spherical-averaged exchange hole (or particle) density with the counterpart in the static limit that is also known as Hatree-Fock approximation (HFA). To quantify the degree of deviation of the exchange in our formalism with HFA, we define degree of the deviation as follows:

$$\delta\bar{\rho}_{\mathrm{x}} = \int dR' \left| \bar{\rho}_{\mathrm{x}}(R, R', R''; t < 0) - \bar{\rho}_{\mathrm{x}}(R = 0, R', R'' = R'; t = 0) \right|, \tag{2.45}$$

where the integral on the right-hand side is performed over a specific range of R'.

2.4 Formula for the 3D HEG

To avoid any confusion, all the results and plots in 3D are expressed in atomic units (a.u.) and correspond to $r_s = 4$.

In 3D, Eq. (2.43) becomes

$$\begin{aligned} iG_0(R; t) =& \frac{1}{2\pi^2 R} \int_{k_{\mathrm{F}}}^{\infty} dk\, k \sin(kR) e^{-ik^2 t/2} \theta(t) \\ & - \frac{1}{2\pi^2 R} \int_0^{k_{\mathrm{F}}} dk\, k \sin(kR) e^{-ik^2 t/2} \theta(-t). \end{aligned} \tag{2.46}$$

The expression of the exchange hole ($t < 0$) is simplified

$$\rho_{\mathrm{x}}(R, R', R''; t < 0) = -\frac{1}{2\pi^2} \frac{1}{R^3} \frac{[\sin(k_{\mathrm{F}}R') - k_{\mathrm{F}}R' \cos(k_{\mathrm{F}}R')] \int_0^{k_{\mathrm{F}}} dk\, k \sin(kR'') e^{-ik^2 t/2}}{\int_0^{k_{\mathrm{F}}} dk\, k \sin(kR) e^{-ik^2 t/2}}, \tag{2.47}$$

and the exchange particle ($t > 0$) is given by

$$\rho_{\mathrm{x}}(R, R', R''; t > 0) = -\frac{1}{2\pi^2} \frac{1}{R^3} \frac{[\sin(k_{\mathrm{F}}R') - k_{\mathrm{F}}R' \cos(k_{\mathrm{F}}R')] \int_{k_{\mathrm{F}}}^{\infty} dk\, k \sin(kR'') e^{-ik^2 t/2}}{\int_{k_{\mathrm{F}}}^{\infty} dk\, k \sin(kR) e^{-ik^2 t/2}}, \tag{2.48}$$

in which form the property

$$\rho_{\rm x}(R,R',R;t)=-\rho(R')$$

becomes obvious.

The exchange potential has a relatively simple form due to the fact that the radial component of one of momenta is analytically solvable. Using the result from the well-known static Lindhard function [6]

$$f(k)=\frac{k_{\rm F}}{2\pi^2}\left(\frac{1}{2}+\frac{k_{\rm F}^2-k^2}{4k_{\rm F}k}\ln\left|\frac{k_{\rm F}+k}{k_{\rm F}-k}\right|\right), \tag{2.49}$$

the exchange potential for $t<0$ is given by

$$V_{\rm x}(R;t<0)=\frac{1}{iG_0(R;t<0)}\times\frac{2}{\pi R}\int_0^{k_{\rm F}}dk\ k\sin(kR)\ e^{-i\varepsilon_k t}f(k). \tag{2.50}$$

Conversely, it is given by

$$V_{\rm x}(R;t>0)=-\frac{1}{iG_0(R;t>0)}\times\frac{2}{\pi R}\int_{k_{\rm F}}^{\infty}dk\ k\sin(kR)\ e^{-i\varepsilon_k t}f(k). \tag{2.51}$$

On the other hand, by following the same strategy, one could obtain the expressions for correlation hole and particle in terms of four similar terms. To determine them, however, there remains 5-dimensional integral to be carried out even after simplification based on the angular symmetry, which makes it too expensive to calculate.

Instead, the spherical-averaged density and potential, thanks to the extra polar angle integral decoupling the original two polar angles, can be expressed relatively simply as 4-dimensional integrals with neat integrands.

The relevant terms of spherical-averaged correlation density are given by

$$\begin{aligned}\bar{A}_1=&\frac{1}{2\pi^3R}\int_{k_{\rm F}}^{\infty}dk'\ k'\sin(k'R)\int_0^{k_{\rm F}}dk\ k^2e^{-i\varepsilon_k t}\\&\times\int_{-1}^{1}dy\frac{\sin(qR')}{qR'}M(q,\varepsilon_{k'}-\varepsilon_k;t);\end{aligned} \tag{2.52}$$

$$\begin{aligned}\bar{A}_2=&\frac{1}{2\pi^3R}\int_{k_{\rm F}}^{\infty}dk\ k\sin(kR)\int_0^{k_{\rm F}}dk'\ k'^2e^{-i\varepsilon_{k'}t}\\&\times\int_{-1}^{1}dy\frac{\sin(qR')}{qR'}M(q,\varepsilon_k-\varepsilon_{k'},0);\end{aligned} \tag{2.53}$$

$$\begin{aligned}\bar{B}_1=&\frac{1}{2\pi^3R}\int_{k_{\rm F}}^{\infty}dk'\ k'\sin(k'R)e^{-i\varepsilon_{k'}t}\int_0^{k_{\rm F}}dk\ k^2\\&\times\int_{-1}^{1}dy\frac{\sin(qR')}{qR'}M(q,\varepsilon_{k'}-\varepsilon_k,0);\end{aligned} \tag{2.54}$$

$$\bar{B}_2 = \frac{1}{2\pi^3 R}\int_{k_\mathrm{F}}^{\infty} dk\ k\sin(kR)e^{-i\varepsilon_k t}\int_0^{k_\mathrm{F}} dk'\ k'^2 \times \int_{-1}^{1} dy \frac{\sin(qR')}{qR'} M(q, \varepsilon_k - \varepsilon_{k'}, -t), \tag{2.55}$$

where

$$q = |\mathbf{k}' - \mathbf{k}| = \sqrt{k'^2 + k^2 - 2k'ky}, \qquad y = \cos\alpha. \tag{2.56}$$

To obtain the correlation potential, the first moment of spherical-averaged correlation density should be integrated from $R' = 0$ to $R' = \infty$, which can be carried out analytically,

$$\int_0^{\infty} dR'\ \sin(qR') = \frac{1}{q}. \tag{2.57}$$

Equivalently, one can directly replace $\frac{\sin(qR')}{qR'}$ with $\frac{1}{q^2}$.

After constructing all the kinematic part, it is time to add the dynamics.

Recall the content of $M(q, \omega; t)$ in Eq. (2.41) and Eq. (2.35), and $K(k, \omega)$ is given by

$$K(q, \omega) = v(q)\chi(q, \omega), \tag{2.58}$$

where $\chi(q, \omega)$ is the the RPA response function in Eq. (2.18), $L(q, \omega)$ can be expressed as

$$L(q, \omega) = -\frac{1}{\pi}\mathrm{sign}(\omega)\frac{v(q)\mathrm{Im}P_0(q, \omega)}{(1 - v(q)\mathrm{Re}P_0(q, \omega))^2 + (v(q)\mathrm{Im}P_0(q, \omega))^2}. \tag{2.59}$$

More conventionally, by defining the dynamical dielectric function

$$\epsilon(q, \omega) = 1 - v(q)P_0(q, \omega), \tag{2.60}$$

it can be expressed alternatively as

$$L(q, \omega) = -\frac{1}{\pi}\mathrm{sign}(\omega)\mathrm{Im}\epsilon^{-1}(q, \omega). \tag{2.61}$$

Since $P_0(q, \omega)$ is the polarization in the RPA that is known as Lindhard function, Eq. (2.60) is recognized as the well-known the RPA dielectric function.

In the unit of k_F for momentum and $2\varepsilon_F = k_F^2$ for energy (frequency), by making use of Eq. (2.21), one obtains [9, 10]

$$\mathrm{Re}P_0(q, \omega) = \frac{k_\mathrm{F}}{2\pi^2}\Big\{-1 + \frac{1}{2q}\left[1 - \left(\frac{\omega}{q} - \frac{q}{2}\right)^2\right]\ln\left|\frac{1 + (\omega/q - \frac{1}{2}q)}{1 - (\omega/q - \frac{1}{2}q)}\right| - \frac{1}{2q}\left[1 - \left(\frac{\omega}{q} + \frac{q}{2}\right)^2\right]\ln\left|\frac{1 + (\omega/q + \frac{1}{2}q)}{1 - (\omega/q + \frac{1}{2}q)}\right|\Big\}; \tag{2.62}$$

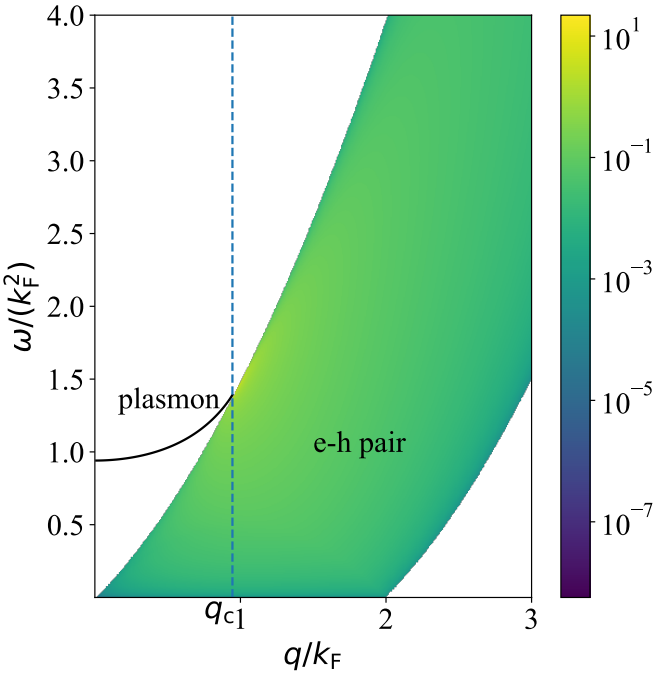

Figure 2: Heatmap of $L(q,\omega)$ for the 3D HEG, where the plasmon is the black solid line.

$$\mathrm{Im}P_0(q,\omega) = \begin{cases} -\frac{k_\mathrm{F}}{4\pi q}\left[1-\left(\frac{\omega}{q}-\frac{1}{2}q\right)^2\right], & (q\geq 2,\ \frac{q^2}{2}+q\geq\omega\geq\frac{q^2}{2}-q) \\ -\frac{k_\mathrm{F}}{4\pi q}\left[1-\left(\frac{\omega}{q}-\frac{1}{2}q\right)^2\right], & (q<2,\ -\frac{q^2}{2}+q\leq\omega\leq\frac{q^2}{2}+q) \\ -\frac{k_\mathrm{F}}{2\pi}\frac{\omega}{q}, & (q<2,\ 0\leq\omega\leq-\frac{q^2}{2}+q) \\ 0, & \text{otherwise} \end{cases} \tag{2.63}$$

There exist two regions where $L(q,\omega)$ does not vanish. One is where $\mathrm{Im}P_0(k,\omega)\neq 0$, the other is the so called plasmon branch, where $\mathrm{Im}P_0(q,\omega)=0$ while $1-v(q)\mathrm{Re}P_0(q,\omega)=0$ as well, so that $L(q,\omega)\neq 0$ (see Figure 2). It can be seen that beyond a critical momentum $q_\mathrm{c}\approx 0.945k_\mathrm{F}$, the plasmon is mixed with electron-hole (e-h) pairs. According to the colour bar in the Figure 2, the lighter the colour is, the bigger the $L(q,\omega)$ is. The response fluctuation is drastic around the tail of the plasmon branch, showcasing the effect of the presence of a collective plasmon mode.

2.5 Formula for the 2D HEG

To circumvent any confusion, all the results and plots are expressed in atomic units (a.u.) and correspond to $r_s = 10$ that is a typical value for 2D materials.

In 2D, Eq. (2.43) becomes

$$\begin{aligned} iG_0(R;t) =& \frac{1}{2\pi}\int_{k_\mathrm{F}}^{\infty} dk\, k e^{-ik^2t/2} J_0(kR)\theta(t) \\ & - \frac{1}{2\pi}\int_{0}^{k_\mathrm{F}} dk\, k e^{-ik^2t/2} J_0(kR)\theta(-t), \end{aligned} \tag{2.64}$$

where $J_0(kR)$ is the Bessel function of the first kind of the 0th order. By making use of the series expansion of J_0

$$J_0(x) = \sum_{m=0}^{\infty} \frac{(-1)^m}{(m!)^2}\left(\frac{x}{2}\right)^{2m}, \tag{2.65}$$

and making variable transformation $y = k^2$, one can perform the integration and get

$$iG_0(R;t<0) = -\frac{1}{2\pi}\frac{1}{2}\sum_{m=0}^{\infty}\frac{(-1)^m}{(m!)^2}\left(\frac{R}{2}\right)^{2m} F_m, \tag{2.66}$$

where

$$F_m = \int_0^{k_\mathrm{F}^2} dy\; e^{-\beta y} y^m \tag{2.67}$$

and $\beta = it/2$. Integration by part yields the recursion relation

$$F_m = \frac{1}{\beta}\left(mF_{m-1} - k_\mathrm{F}^{2m} e^{-\beta k_\mathrm{F}^2}\right) \tag{2.68}$$

with

$$F_0 = \frac{1}{\beta}\left(1 - e^{-\beta k_F^2}\right). \tag{2.69}$$

Then the general expression can be obtained

$$F_m = \frac{1}{\beta^{m+1}} m!\left(1 - e^{-\beta k_F^2}\right) - \sum_{n=1}^{m} n!\left(\frac{k_F^2}{\beta}\right)^n e^{-\beta k_F^2}. \tag{2.70}$$

For $t > 0$, the non-interacing Green function is given by

$$iG_0(R;t>0) = \frac{1}{2\pi}\frac{1}{2}\sum_{m=0}^{\infty}\frac{(-1)^m}{(m!)^2}\left(\frac{R}{2}\right)^{2m} I_m, \tag{2.71}$$

where

$$I_m = \lim_{\eta \to 0^+} \int_{k_{\rm F}^2}^{\infty} dy\, e^{(-\beta+\eta)y} y^m, \tag{2.72}$$

where a convergent factor is multiplied to guarantee the convergence in infinity. The corresponding recursion relation is

$$I_m = \frac{1}{\beta}\left(m I_{m-1} + k_{\rm F}^{2m} e^{-\beta k_{\rm F}^2} \right), \tag{2.73}$$

and the general expression is

$$I_m = \frac{1}{\beta^{m+1}} m! \left(1 - e^{-\beta k_F^2} \right) + \sum_{n=1}^{m} n! \left(\frac{k_F^2}{\beta} \right)^n e^{-\beta k_F^2}. \tag{2.74}$$

In particular, for $t = 0^-$,

$$iG_0(R; t = 0^-) = -\frac{1}{(2\pi)^2} \frac{1}{2} \sum_{m=0}^{\infty} \frac{(-1)^m}{(m!)^2} \left(\frac{R'}{2} \right)^{2m} \frac{k_{\rm F}^{2(m+1)}}{2m+1}. \tag{2.75}$$

The exchange potential is given by

$$V_x(R; t) = \frac{1}{iG_0(R; t)} \int_0^{k_{\rm F}} dk\ k e^{-i\varepsilon_k t} J_0(kR) f(k), \tag{2.76}$$

where

$$f(k) = \frac{1}{(2\pi)^2} \int_0^{k_{\rm F}} dk' k' \frac{4}{(k'+k)} \mathbf{K}\left(\frac{2\sqrt{kk'}}{k+k'} \right), \tag{2.77}$$

and

$$\mathbf{K}\left(\frac{2\sqrt{kk'}}{k+k'} \right) = \frac{(k'+k)}{4} \int_0^{2\pi} d\theta \frac{1}{\sqrt{k'^2 + k^2 - 2kk' \cos\theta}} \tag{2.78}$$

is one of the expression of the complete elliptic integral of the first kind. As in 3D, the spherical-averaged correlation hole and potential are essentially expressible in the following four terms:

$$\begin{aligned} \bar{A}_1 = & \int_{k_{\rm F}}^{\infty} dk'\ k' J_0(k'R) \int_0^{k_{\rm F}} dk\ k e^{-i\varepsilon_k t} \\ & \times \int_0^{2\pi} d\alpha\ J_0(qR') M(q, \varepsilon_{k'} - \varepsilon_k; t); \end{aligned} \tag{2.79}$$

$$\bar{A}_2 = \int_{k_F}^{\infty} dk\ kJ_0(kR) \int_0^{k_F} dk'\ k' e^{-i\varepsilon_{k'}t} \times \int_0^{2\pi} d\alpha\ J_0(qR')M(q, \varepsilon_k - \varepsilon_{k'}, 0); \tag{2.80}$$

$$\bar{B}_1 = \int_{k_F}^{\infty} dk'\ k' J_0(k'R) e^{-i\varepsilon_{k'}t} \int_0^{k_F} dk\ k \times \int_0^{2\pi} d\alpha\ J_0(qR')M(q, \varepsilon_{k'} - \varepsilon_k, 0); \tag{2.81}$$

$$\bar{B}_2 = \int_{k_F}^{\infty} dk\ kJ_0(kR) e^{-i\varepsilon_k t} \int_0^{k_F} dk'\ k' \times \int_0^{2\pi} d\alpha\ J_0(qR')M(q, \varepsilon_k - \varepsilon_{k'}, -t), \tag{2.82}$$

As in the 3D HEG, the first moment of the spherical-averaged correlation density should be integrated to calculate the potential and equivalently it could be done by replacing $J_0(qR')$ with $\frac{1}{q}$.

Similarly, in 2D, the polarization is given by

$$\mathrm{Re}P_0(q,\omega) = \frac{1}{\pi}\Bigg[-1-\mathrm{sign}(2\omega - q^2)\theta[|2\omega - q^2|/(2q) - 1]\frac{1}{q}\sqrt{\left|\frac{2\omega - q^2}{2q}\right|^2 - 1} + \mathrm{sign}(2\omega + q^2)\theta[|2\omega + q^2|/(2q) - 1]\frac{1}{q}\sqrt{\left|\frac{2\omega + q^2}{2q}\right|^2 - 1}\Bigg] \tag{2.83}$$

$$\mathrm{Im}P_0(q,\omega) = \begin{cases} -\frac{1}{\pi}\frac{1}{q}\sqrt{1 - \frac{1}{4}\left(\frac{2\omega}{q} - q\right)^2}, & (q > 2,\ \frac{q^2}{2} + q \geq \omega \geq \frac{q^2}{2} - q) \\ -\frac{1}{\pi}\frac{1}{q}\sqrt{1 - \frac{1}{4}\left(\frac{2\omega}{q} - q\right)^2}, & (q < 2,\ -\frac{q^2}{2} + q \leq \omega \leq \frac{q^2}{2} + q) \\ -\frac{1}{\pi}\frac{1}{q}\Bigg[\sqrt{1 - \frac{1}{4}\left(\frac{2\omega}{q} - q\right)^2} & \\ -\sqrt{\left(1 - \frac{q^2}{4}\right) - \omega - \frac{\omega^2}{q^2}}\Bigg], & (q < 2,\ 0 \leq \omega \leq -\frac{q^2}{2} + q) \\ 0, \quad \text{otherwise} & \end{cases} \tag{2.84}$$

There is also a plasmon-excitation in 2D (see Figure 3). However, it is not mixed with electron-hole pairs at all (see Figure 4). Instead, it has a critical momentum $k_c \approx 3.543296$, and the corresponding energy is beyond the e-h pair constraint $k_c^2/2 + k_c$. This is a unique feature of 2D electron gas. Also, unlike the 3D case, in the limit of long wavelength, i.e. $q \to 0$, the 2D electron gas does not sustain a plasmon.

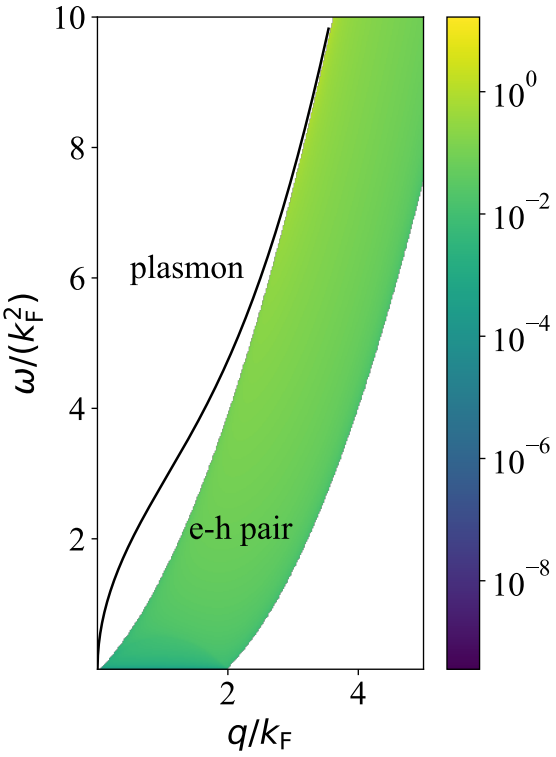

Figure 3: Heatmap of $L(k, \omega)$ for the 2D HEG, where the plasmon branch is the black solid line.

2.6 dD Hubbard cubic lattice in the RPA

The Hamiltonian of Hubbard model including only nearest-neighbor hopping with periodic boundary condition is given by

$$\hat{H} = -T \sum_{i<j} \sum_{\sigma} (\hat{c}^{\dagger}_{i\sigma} \hat{c}_{j\sigma} + \text{H.c.}) + U \sum_{i} \hat{n}_{i\uparrow} \hat{n}_{i\downarrow}. \tag{2.85}$$

Since there is no analytical solution guaranteed for the Hubbard model in arbitrary size except for 1D case, it has to resort to certain approximation such as the RPA. We focus on the cubic lattice with separation a. The noninteracting Green function is given by

$$G^0(r, r'; t) = i\theta(-t) \sum_{\mathbf{k}}^{\text{occ}} \varphi_{\mathbf{k}}(r) \varphi^*_{\mathbf{k}}(r') e^{-i\varepsilon_{\mathbf{k}} t} - i\theta(t) \sum_{\mathbf{k}'}^{\text{unocc}} \varphi_{\mathbf{k}'}(r) \varphi^*_{\mathbf{k}'}(r') e^{-i\varepsilon_{\mathbf{k}'} t}, \tag{2.86}$$

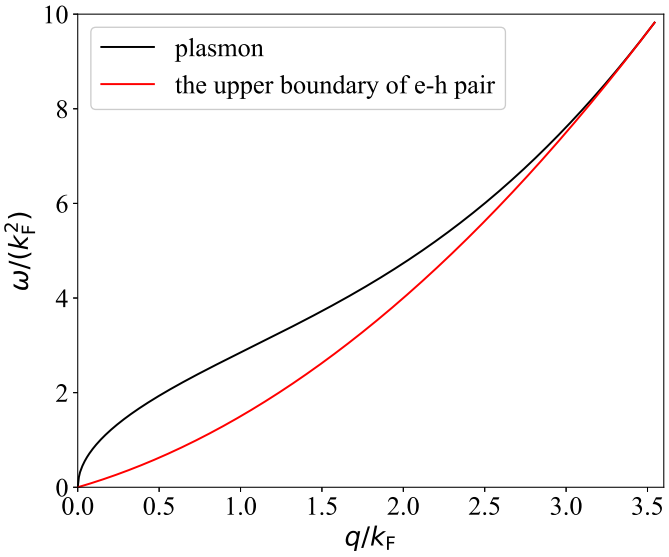

Figure 4: Dispersion of the plasmon excitation (black) and the upper boundary of electron-hole pair excitation (red) for the 2D HEG.

where $\varphi_{\mathbf{k}}$ and $\varphi_{\mathbf{k}'}$ are the spin-independent occupied and unoccupied Bloch states,

$$\varphi_{\mathbf{k}} = \frac{1}{\sqrt{N}} \sum_j e^{i\mathbf{k}\cdot\mathbf{R_j}} \varphi_j(r), \tag{2.87}$$

where N is the number of sites.

Recalling Eq. (2.7), the product in the form $\rho_{\mathrm{xc}} G^0$ in the real space will be a matrix element $(\rho_{\mathrm{xc}} G^0)_{nm}$ in the basis given by Eq. (2.87). The exchange part is given by

$$\begin{aligned} (\rho_{\mathrm{x}} G^0)_{nm} =& \rho_{\mathrm{x}}^{nm} G^0_{mm} \\ =& -i \varphi^*_{\mathbf{k}_n}(r'') \varphi_{\mathbf{k}_m}(r'') e^{-i\varepsilon_{\mathbf{k}_m} t}, \end{aligned} \tag{2.88}$$

from which the nm component of exchange hole can be obtained

$$\rho_{\mathrm{x}}^{nm} = \begin{cases} -\varphi^*_{\mathbf{k}_n}(r'') \varphi_{\mathbf{k}_m}(r''), & \mathbf{k}_n, \mathbf{k}_m \in \text{occ} \\ 0. & \text{otherwise} \end{cases} \tag{2.89}$$

Based on this result, the matrix element $(V_{\mathrm{x}} G^0)_{nm}$ is given by

$$(V_{\mathrm{x}} G^0)_{nm} = -i \frac{U N_{\mathrm{occ}}}{N} \delta_{n,m} e^{-i\varepsilon_{\mathbf{k}_m} t}, \tag{2.90}$$

where N_{occ} denotes the total number of spin-independent occupied Bloch states. It can be simplified further by making use of the content of the Green function

$$\sum_{\mathbf{k}_l}^{\text{occ}} V_{\text{x}}^{ml,lm} e^{-i\varepsilon_{\mathbf{k}_l} t} = \begin{cases} -\frac{UN_{\text{occ}}}{N} e^{-i\varepsilon_{\mathbf{k}_m} t}, & \mathbf{k}_m \in \text{occ} \\ 0. & \text{otherwise} \end{cases} \tag{2.91}$$

For a specific finite lattice, it is possible to solve out V_{x} in principle. Similarly, for $t > 0$,

$$\rho_{\text{x}}^{nm} = \begin{cases} -\varphi_{\mathbf{k}_n}^*(r'')\varphi_{\mathbf{k}_m}(r''), & \mathbf{k}_n \in \text{occ}, \mathbf{k}_m \in \text{unocc} \\ 0, & \text{otherwise} \end{cases} \tag{2.92}$$

and

$$\sum_{\mathbf{k}_l}^{\text{unocc}} V_{\text{x}}^{ml,lm} e^{-i\varepsilon_{\mathbf{k}_l} t} = \begin{cases} -\frac{UN_{\text{occ}}}{N} e^{-i\varepsilon_{\mathbf{k}_m} t}, & \mathbf{k}_m \in \text{unocc} \\ 0. & \text{otherwise} \end{cases} \tag{2.93}$$

For the correlation part, it is a bit more complicated than exchange part, so that all the derivation is put in the Appendix. A. Because the results for the potential are much simpler than the ones for the density, only the latter are listed below. For $t < 0$,

$$\sum_{\mathbf{k}_i} V_{\text{c}}^{mi,im} e^{-i\varepsilon_{\mathbf{k}_i} t} = \sum_{\mathbf{k}_j}^{\text{occ}} \sum_{\mathbf{k}_l}^{\text{unocc}} \alpha_{jl} \frac{U^2}{N^2} \begin{cases} -\frac{e^{-i(\varepsilon_{\mathbf{q}} - \Delta_{lj})t}}{\varepsilon_{\mathbf{q}} - \Delta_{lj} - \varepsilon_{\mathbf{k}_m}}, & \mathbf{k}_m \in \text{unocc} \\ \frac{e^{-i\varepsilon_{\mathbf{k}_m} t}}{\varepsilon_{\mathbf{q}'} + \Delta_{lj} - \varepsilon_{\mathbf{k}_m}}, & \mathbf{k}_m \in \text{occ} \end{cases} \tag{2.94}$$

where

$$\Delta_{hi} = \sqrt{(\Delta_{hi}^0)^2 + \frac{4U}{N}\Delta_{hi}^0}, \quad \alpha_{hi} = \frac{2\Delta_{hi}^0}{\Delta_{hi}},$$

$$\mathbf{q} = \mathbf{k}_m + \mathbf{k}_l - \mathbf{k}_j - \frac{2\pi}{a}\hat{\mathbf{v}}, \quad \mathbf{q}' = \mathbf{k}_m + \mathbf{k}_l - \mathbf{k}_j, \tag{2.95}$$

and

$$\Delta_{hi}^0 = \varepsilon_{\mathbf{k}_h} - \varepsilon_{\mathbf{k}_i}, \quad \hat{\mathbf{v}} = a\sum_{i=1}^{d} \hat{\mathbf{x}}_i. \tag{2.96}$$

Here $\hat{\mathbf{x}}_i$ denotes the unit vector along the ith direction.

Conversely,

$$\sum_{\mathbf{k}_i} V_{\text{c}}^{mi,im} e^{-i\varepsilon_{\mathbf{k}_i} t} = -\sum_{\mathbf{k}_j}^{\text{occ}} \sum_{\mathbf{k}_l}^{\text{unocc}} \alpha_{jl} \frac{U^2}{N^2} \begin{cases} \frac{e^{-i(\varepsilon_{\mathbf{q}'} + \Delta_{lj})t}}{\varepsilon_{\mathbf{p}'} + \Delta_{lj} - \varepsilon_{\mathbf{k}_m}}, & \mathbf{k}_m \in \text{occ} \\ -\frac{e^{-i\varepsilon_{\mathbf{k}_m} t}}{\varepsilon_{\mathbf{q}} - \Delta_{lj} - \varepsilon_{\mathbf{k}_m}}, & \mathbf{k}_m \in \text{unocc} \end{cases} \tag{2.97}$$

3 Results for the 3D HEG

3.1 The correlation potential in the full the RPA

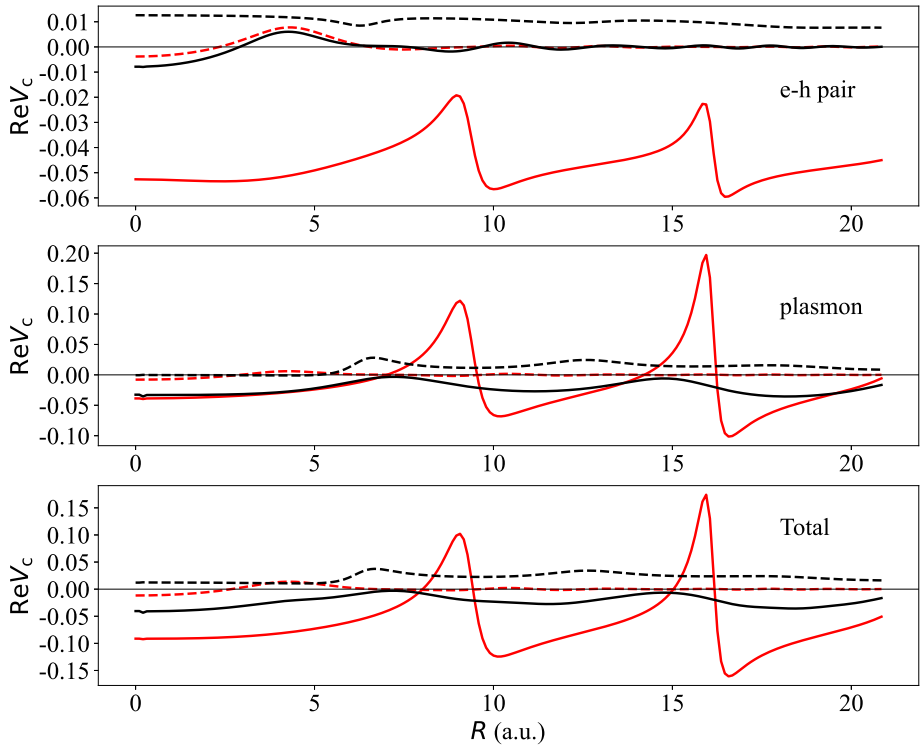

Figure 5: The real parts of the correlation hole given by the electron-hole pair (top), the plasmon (middle), and the total (bottom) for $t = \pm 4.62$ (red) and ± 34.75 (black). The solid and dashed curves correspond to $t < 0$ and $t > 0$, respectively.

Mathematically, the occurrence of a plasmon corresponds to a division 0/0, which is finite but unresolved by the computer so that has to be handled analytically. The dispersion of plasmon is given by two equations at the end of Sect. 2.4, which gives the energy for a specific momentum:

$$\begin{aligned} \epsilon_1(q,\omega) =& 1 - v(q)\mathrm{Re}P_0(q,\omega) = 0 \\ \epsilon_2(q,\omega) =& \mathrm{Im}P_0(q,\omega) = 0. \end{aligned} \tag{3.1}$$

By Taylor expanding $\mathrm{Re}\epsilon_0(k,\omega)$ in powers of ω around the plasmon energy Ω_k to the first

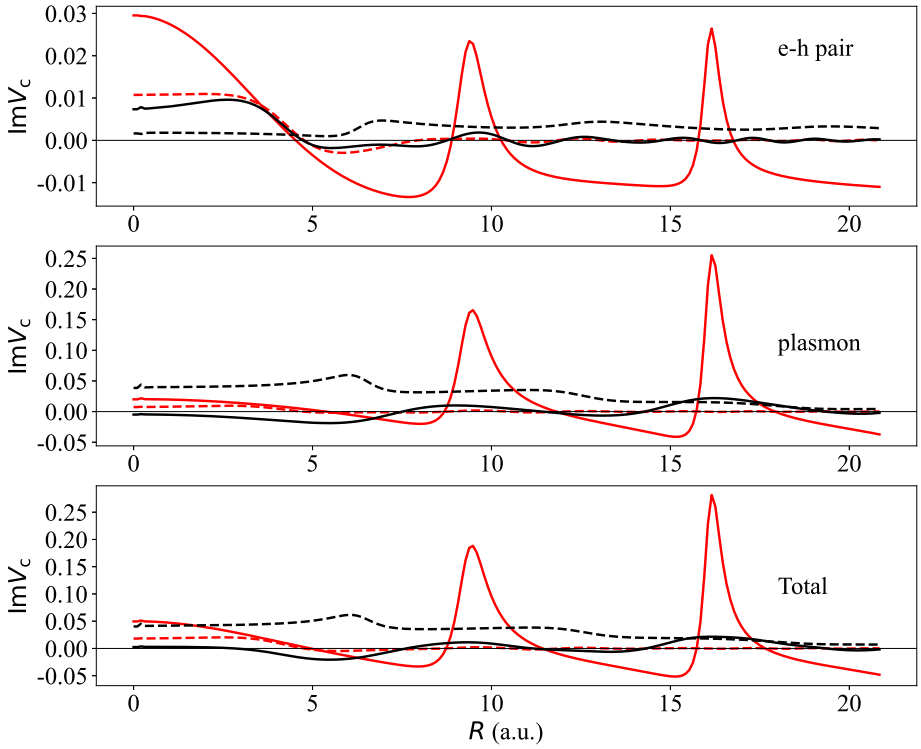

Figure 6: The imaginary parts of the correlation potential given by the electron-hole pair (top), the plasmon (middle), and the total (bottom) for $t = \pm 4.62$ (red) and ± 34.75 (black). The solid and dashed curves correspond to $t < 0$ and $t > 0$, respectively.

order,

$$\begin{aligned}\varepsilon_1(q,\omega) =& \varepsilon_1(q,\Omega_q) + (\omega - \Omega_q)\frac{\partial \varepsilon_1(q,\omega)}{\partial \omega}\Big|_{\omega=\Omega_q} + \dots \\ =& (\omega - \Omega_q)\frac{\partial \varepsilon_1(q,\omega)}{\partial \omega}\Big|_{\omega=\Omega_q},\end{aligned} \tag{3.2}$$

where the 0th order term vanishes because of Eq. (3.1). Then by Hilbert transformation, one obtains the imaginary part of inverse dielectric function around the plasmon energy

$$\mathrm{Im}\epsilon^{-1}(\omega) = \frac{1}{\epsilon_1'(\Omega_q)}\delta(\omega - \Omega_q), \tag{3.3}$$

where

$$\epsilon_1'(\Omega_q) = \frac{\partial \varepsilon_1(q,\omega)}{\partial \omega}\Big|_{\omega=\Omega_q 0w}. \tag{3.4}$$

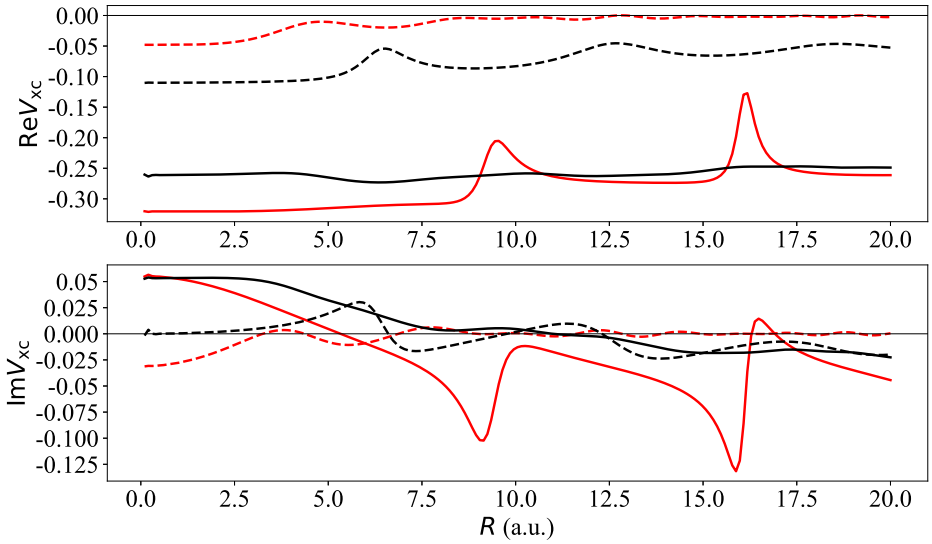

Figure 7: The real and imaginary parts of the exchange-correlation potential for $t = \pm 4.62$ (red) and ± 34.75 (black). The solid and dashed curves correspond to $t < 0$ and $t > 0$, respectively.

In practice, the delta function is approximated by a certain function such as Lorentzian function or Gaussian function with a proper broadening factor. By doing so, the real and imaginary part of the correlation potential for $t = \pm 4.62$ and ± 34.75 are shown in Figure 5 and 6, respectively. Apart from the curve at $t = -4.62$, it can be seen that other potentials vary with distance only weakly. The strong structure at $t = -4.62$ again, are caused by the local minimum of $|G_0(R;t)|$.

Since the hole and electron carry opposite charges for the Coulomb interaction, the relative position of the curves can be correctly understood. For each pair of electron and hole for the same magnitude of time, the correlation potential for $t < 0$ is always more attractive than for $t > 0$ apart from where it hits the minimums of $|G_0(R;t)|$. Also, for both hole and particle, it is less attractive when t is larger. However, it should be understood separately for hole and particle. For the hole, due to the sum rule, it is highly screened by the electrons and this screening tend to smear over time to reach another equilibrium; while for the particle, the screening is not strong so the dominant interaction is the repulsive interaction between electrons. For a large t, this process is performed further so that the corresponding correlation potential is less attractive.

We also note that the total potential is dominated by the plasmon part. The part of the electron-hole (e-h) pair just effectively yields a negative shift and increase the height of peaks. This can find mathematical explanation if we recall how the correlation hole is calculated. The existence of critical momentum for the plasmon restrict the momentum in a

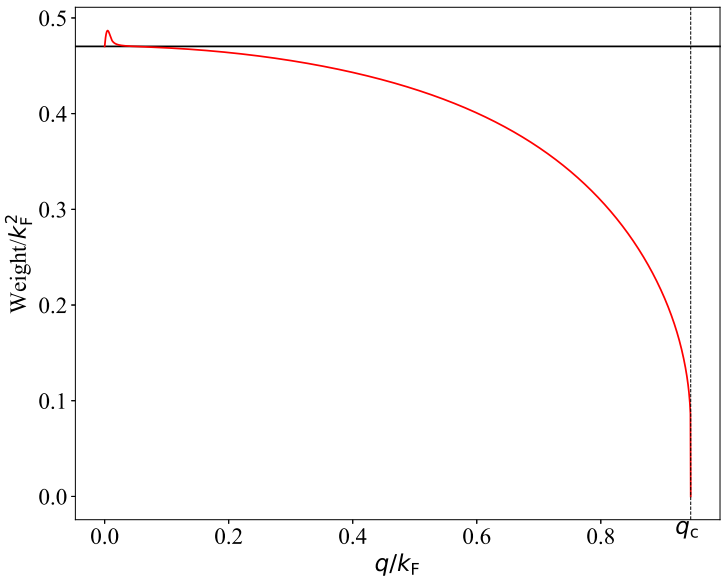

Figure 8: The plasmon weight $1/\epsilon_1'(\Omega_k)$ (red) and its counterpart in the plasmon-pole approximation $\omega/2$ (black) in the range of integration.

small region, which makes the result more sensitive to the change of the spatial separation because of the appearance of R in the sine function. In physics, the appearance of the plasmon mode depends on the singular, long-range nature of Coulomb interaction and it is the long-range interaction contributes most to the screening effect of correlation.

3.2 Comparison with the plasmon-pole approximation

By including the exchange potential, the total exchange-correlation potential is shown in Figure 7. As argued in [6], for the real part, there exist polarization around the Kramers-Kronig-like structures, in which electrons and holes are accumulated in opposite regions where the minimum and maximum of V_x are located. Even within the pole-plasmon approximation, the correlation potential with the opposite structure can somewhat cancel the exchange potential and weaken the polarization. More evidently, this cancellation is reproduced in Figure 7. It can be seen for $t = -34.75$, the fluctuation is almost constant rather than retaining some humps as in the plasmon-pole approximation. However, considering the simplicity of the plasmon-pole approximation, it does not lose its status as a good approximation.

The resemblance between results in the full RPA and those in the plasmon-pole approximation is a consequence of the proper cut-off for the upper limit in the latter. According

to [6], the plasmon-pole approximation is defined as

$$L(k,\omega) = \frac{\omega_p}{2}[\delta(\omega-\omega_p) - \delta(\omega+\omega_p)]. \tag{3.5}$$

In practice, by making used of Eq. (2.36), $w > 0$ can always hold. So only the positive excitation contributes. In the plasmon-pole approximation, there is a cut-off $1.5k_F$ for the upper limit of the integral over momentum of the hole, while it goes up to the $1.02k_F$ here for the plasmon part. Since the correlation potential is dominated by the plasmon, the main difference is caused by the plasmon weight and the plasmon energy are replaced by $\omega_p/2$ and ω_p, respectively. The plasmon weight $1/\epsilon_1'(\Omega_k)$ and the approximation $\omega/2$ are shown in Figure 8. It can be seen when q is close to zero, the approximation is exact as expected. In the full calculations, the plasmon weight is set to zero beyond the critical momentum and all weight is assigned to the e-h pairs, whereas in the plasmon-pole approximation the maximum momentum is chosen to be $1.5k_{\mathrm{F}}$ for $r_s = 4$. As argued at the end of Sect. 3.1, the main contribution to the correlation hole and potential comes from the long-wave length interaction. Also, in Figure 2, slope of the dispersion is actually gentle. These facts explain why the approximation is so good.

4 Results for the 2D HEG

4.1 Exchange hole and potential

4.1.1 Angular dependence of the exchange hole

In Figure 9 the real part of the exchange holes for three cases $t = -5,\ -50,\ -100$ and $R = 10$ are displayed in three subplots from top to bottom. In each subplot, the curves correspond to three different angles $\theta = 0,\ \pi/4,\ \pi/2$, which is the angle between R and R'. The curves should be understood as the density fluctuation induced by the exchange-only interaction, which corresponds to the process a hole created at $R = 0$ at $t < 0$ and annihilated later at $R = 10,\ t = 0$. For $\theta = \pi/2$, it can be seen that the fluctuations are evenly distributed along the orientation of R' as it should be since now either direction is perpendicular to R, which means they are equivalent for this process.

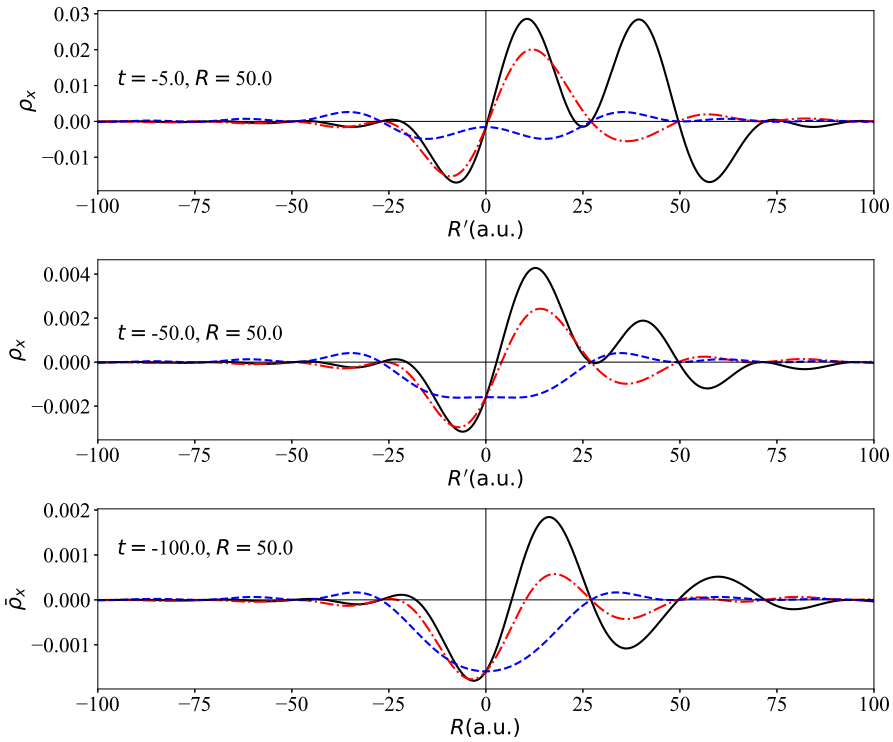

Figure 9: The real part of the exchange hole for $\theta = 0$, (solid black), $\pi/2$ (dashed blue), $\pi/4$ (dotdash red) for the case $R = 50,\ t = -5$ (top), $R = 50,\ t = -50$ (middle) and $R = 50,\ t = -100$ (bottom).

On the contrary, for $\theta = 0$, the fluctuations are stronger in the direction toward $R = 10$ from the origin than in the opposite direction, which reflects the preponderance of the hole

presence and its effect in the former direction. In the comparison of the three cases, the fluctuation along the direction perpendicular to the line joining $R = 0$ and $R = 50$ are found to be the least whereas for the direction $\theta = \pi/4$ they are moderate.

4.1.2 Time dependence of the exchange hole

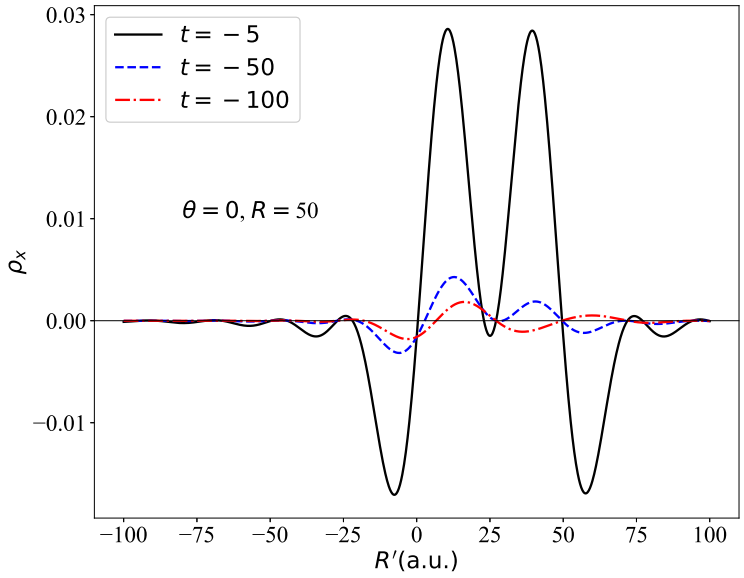

Figure 10: The real parts of the exchange hole for $t = -5$ (solid black), -50 (dashed blue) and -100 (dotdash red) for the case $\theta = 0$ and $R = 50$.

To explore the time dependence of the exchange hole further, the exchange holes for three times $t = -5,\ -50, -100$ are shown in Figure 10 for the case $R = 50$ and $\theta = 0$. It is now more apparent that the fluctuations are much stronger for a short timescale than those of a long period. In particular, for $t = -5$, the fluctuation are almost symmetric about $R' = 25$, which is the center point of the propagation of the created hole. When it comes to $t = -50$, It is no longer symmetric. As for $t = -100$, the fluctuation induced by the creation of a hole still remain there whereas those induced by the annihilation of a hole nearly get relaxed.

One may explain that within a short timescale, the system may not have sufficient time to relax. Based on this explanation, the fluctuations associated with annihilation of the hole or creation of the electron stabilize much faster than those associated with creation of the hole or annihilation of the electron.

This is understandable for exchange interaction because for an electron originally in the

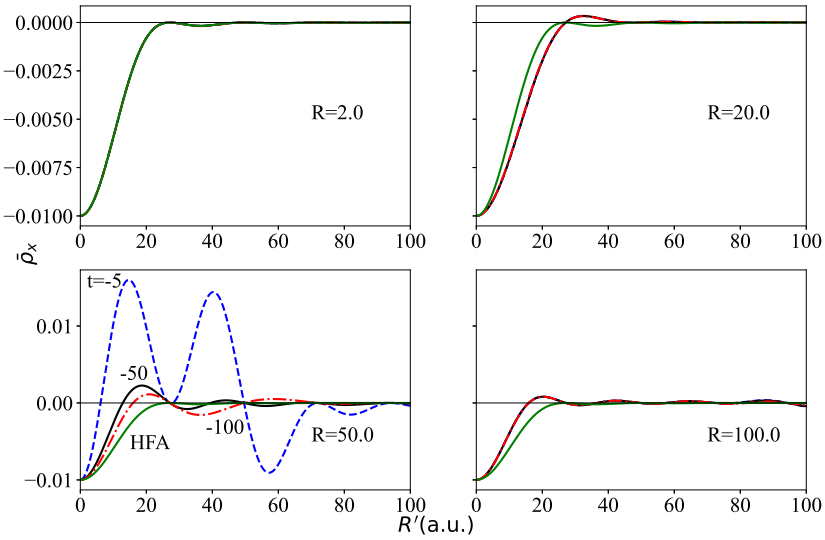

Figure 11: The real part of the spherical average of the exchange hole for $t = -5$ (dashed blue), -50 (solid black) and -100 (dotdash red) for the case $R = 2$ (left top), 20 (right top), 50 (left bottom) and 100 (right bottom). The solid green curve is the static exchange hole from the HFA.

occuipied band (below the Fermi level), if annihilated, definitely induces more fluctuations than when it is created in the unoccupied band (above the Fermi level) since it has more overlap with other electrons, which accounts for such a difference. One may expect the correlation hole has a different behavior.

4.1.3 Spherical average of the exchange hole

In the 2D case, it is the spherical average of the hole that determines the corresponding potential. In Figure 11, the spherical average of the exchange hole is shown for several values of R and t. It can be seen that the dependence of exchange hole on t becomes subtle after being spherically averaged, especially when R is extremely large or small.

One may expect the deviation from the HFA would increase when propagation time t or propagation distance R increases. However, we note that for $R = 50$, it is closer to HF for a longer t; while the distance dependence is a little elusive here. To explore the exact dependence, two reference points are selected as $t = -0.1$ and $R = 0.1$ considering the spherical-averaged exchange hole density is at least continuous, and the degree of deviation is exactly defined at the end of Sect. 2.3.

The imaginary part behaves as expected, whose deviation increases over time and has little dependence on R. However, it is interesting to observe that the real part has little

dependence on time, while there are several striking structures, especially around $R = 28$ and $R = 50$. Since the following peaks are becoming much smaller, it is not surprising that the HFA becomes closer to the dynamical exchange again for a relatively large R in Figure 11. Since the real part of density is responsible for the position of resonance emission or absorption in the spectrum, HF can be good for a big enough R in 2D. To see if it is a generic phenomenon, the same calculation is also performed in 3D.

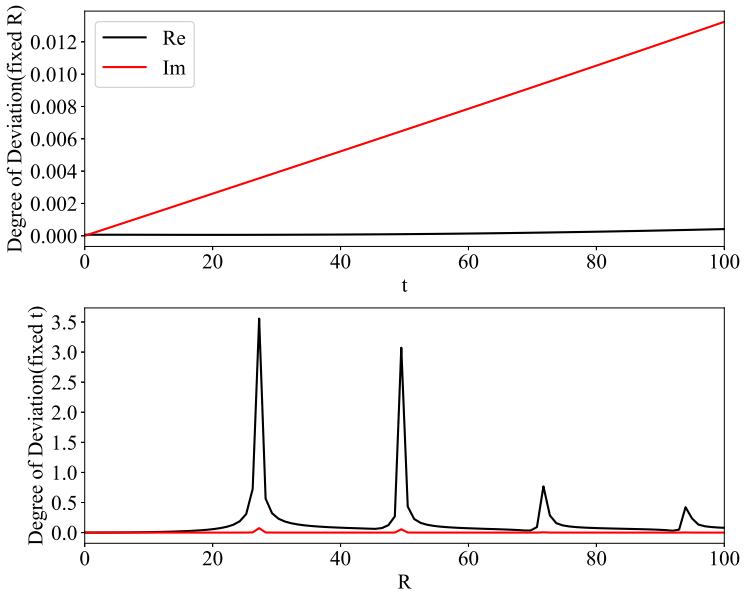

Figure 12: The real (black) and imaginary part (red) of the degree of deviation between the spherical-averaged exchange hole density and its counterpart in HFA over $0 < R' \leq 50$ in the 2D HEG. They are functions of t in the upper panel by fixing R and functions of R in the lower panel by fixing t.

It can be seen the time dependence shows a huge difference from the one in 2D. There is some peak-like structure for both the real and imaginary part. It is not surprising considering the time dependence in the plane wave in the noninteracting Green function. In 2D, it is also the case, but a larger scale of time is needed for such a structure to be observed.

Regarding the dependence on R, we get a similar but much denser structure, but the weight of these peaks do not decrease monotonically. It exhibits two decreasing mode:

1. There is a periodicity for these peaks. Within one period, the weight of peak decreases almost monotonically;

2. The overall weight of each period is smaller than the one of last period.

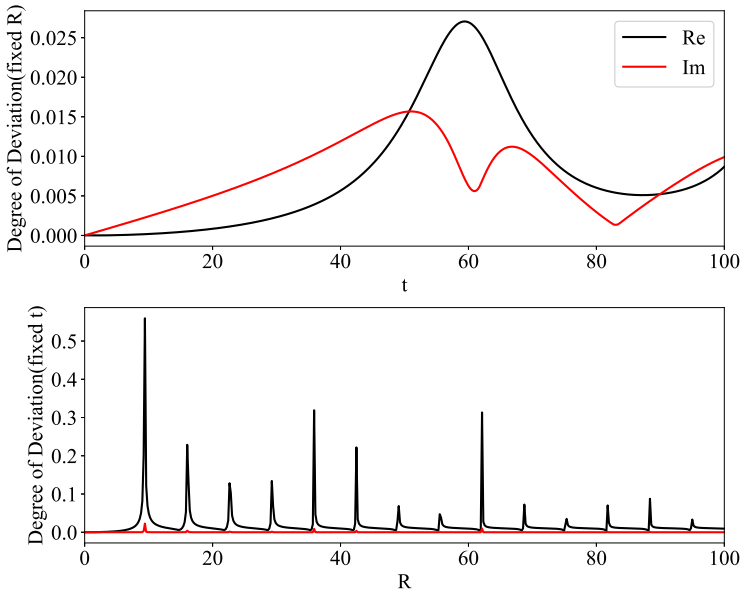

Figure 13: The real (black) and imaginary part (red) of the spherical-averaged exchange hole density and counterpart in HFA over $0 < R' \leq 50$ in the 2D HEG. They are functions of t in the upper panel by fixing R and functions of R in the lower panel by fixing t.

Although this could somewhat explain why the dynamical exchange is closer to the HFA for a larger magnitude of time and a large R rather than for some intermediate values of parameters in Figure 11, we have not found the physical explanation so far. Also, the great deviation for $R = 50$ and $t = -5$ indicates the dependencies on R and t are not independent of each other. Even so, the difference between 2D and 3D is understanable.

Due to the form of noninteracting Green function, t and R only serve as the reciprocal factor of momentum k and energy ε_k of the plane wave, especially in the Bessel function $j_0(kR)$ for 2D, accounting for more cancellation of the integrand since it is more oscillatory. Therefore, there is less deviation from HF for 2D compared to 3D.

On the other hand, because the typical Fermi level in 2D is lower than it in 3D, leading to less cancellation for the hole (t<0) with the Fermi momentum serving as the upper limit of k integrals, which makes it more sensitive to R. From the results we know this feature is not important as it is the Bessel function rather than sine function in 2D.

As a contrast, in Figure 14, the first moment of the spherical average of the exchange hole in 2D is shown. Since this is the quantity that has to be integrated to fulfill the sum rule, it can be observed the fluctuation become more oscillatory than those in Figure 11. Furthermore, the difference gets amplified after being multiplied by R'. For all of the values of R, the spherically averaged fluctuation is strongest for $t = -5$.

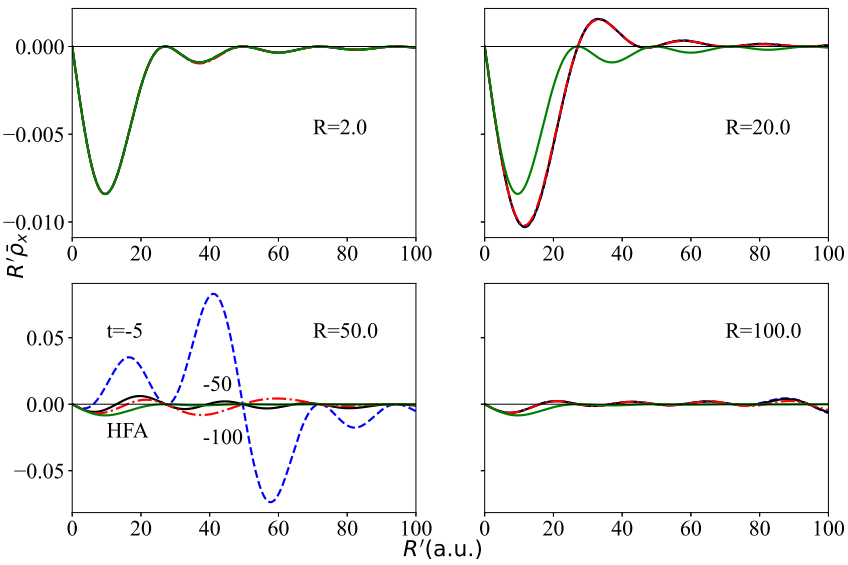

Figure 14: The real part of the first moment of the spherical average of the exchange hole for $t = -5$ (dashed blue), -50 (solid black) and -100 (dashdot red) for the case $R = 2$ (left top), 10 (right top), 30 (left bottom) and 50 (right bottom).

4.1.4 Exchange field

In Figure 15, the real part and imaginary part of the exchange potential for $t = -5$ and -50 are shown. There is striking difference between the exchange potential corresponding to two times. The peaks in the fluctuations is stronger for $t = -4.62$. Physically, the less propagation time for a hole will lead to more drastic density fluctuation, which is the same as in [6]. The position of the peaks are determined by the local minimum of $|G_0(R;t)|$, which can be seen in Figure 16.

Compared to the exchange potential in 3D, it varies more gently overall other than specific places, which reveals the presence of stronger long-range correlation in 2D.

4.2 Correlation hole and potential

The correlation potential for $t = -5$ and -50 are shown in Figure 17 and 18. In our algorithm, $M(|\mathbf{k}' - \mathbf{k}|, \varepsilon_{k'} - \varepsilon_k; t)$ is parameterized as $M(q, \omega)$ and approximated by a two-dimensional interpolation. Due to its non-smooth nature, the interpolation fails to capture subtle details and lead to results with not so high accuracy. Despite of the fact, the results still retain some important features.

The strong structure around $R = 0$ is confusing in the level of either physics or mathe-

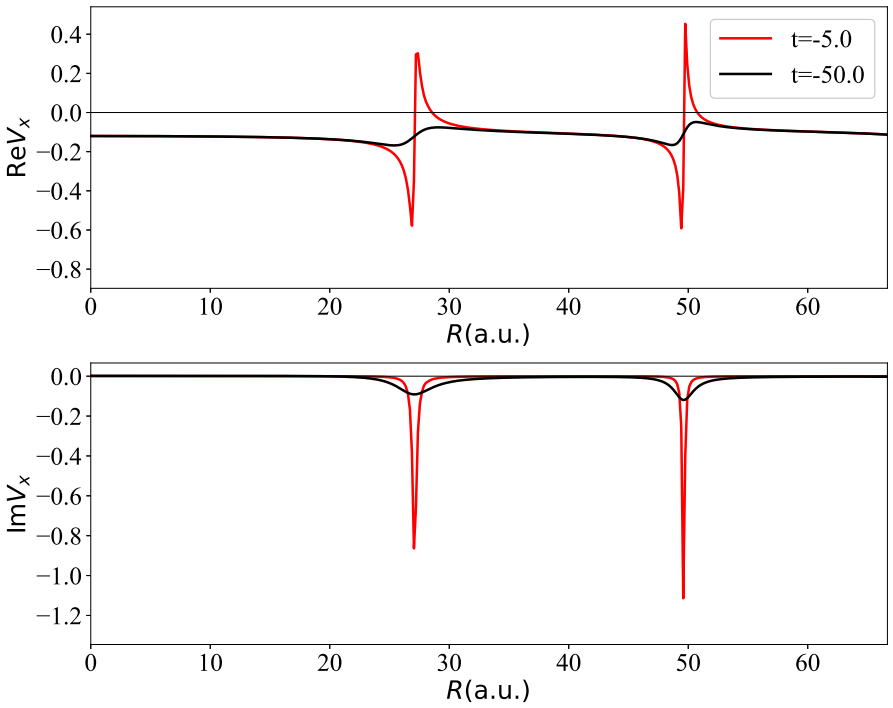

Figure 15: The real part (left) and imaginary part (right) of the exchange potential for $t = -5$ (red) and -50 (blue).

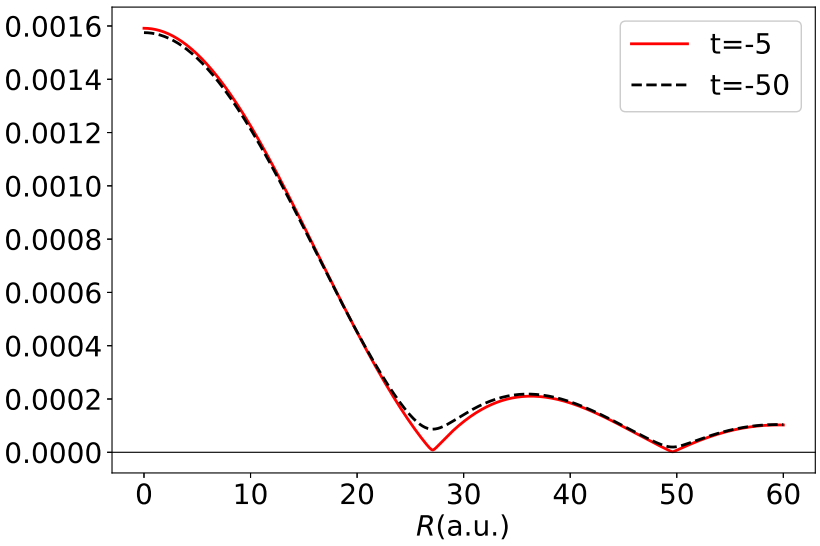

Figure 16: The magnitude of $G_0(R;t)$ for $t = -5$ (solid red) and $t = -50$ (dashed black).

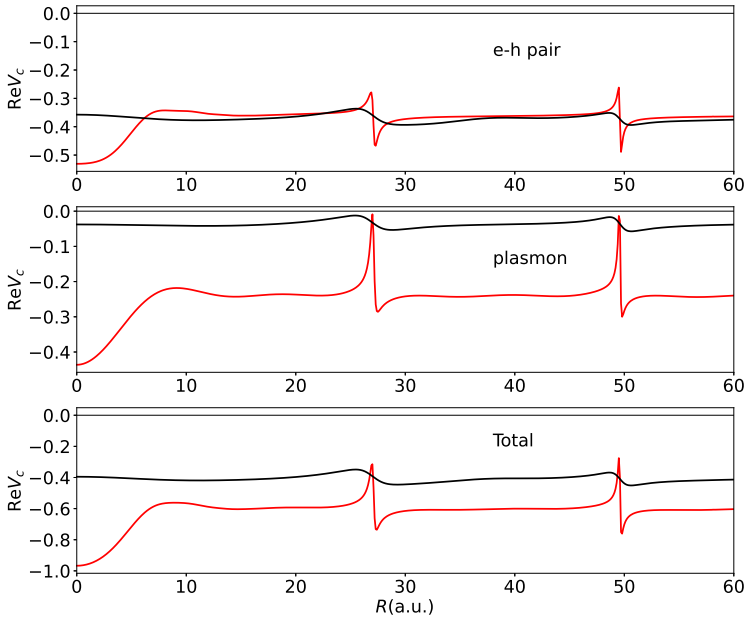

Figure 17: The real parts of the correlation potential given by the electron-hole pair (top), the plasmon (middle), and the total (bottom) for $t = -5$ (red) and -50 (black).

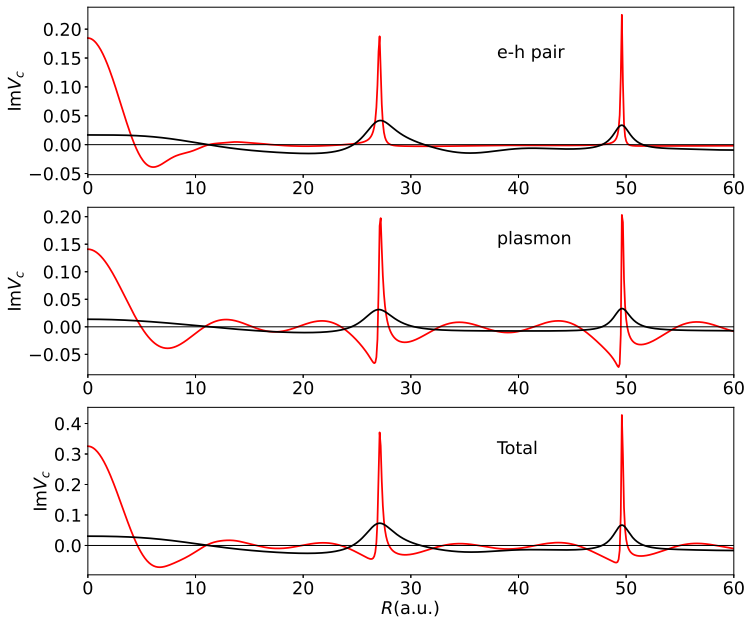

Figure 18: The imaginary parts of the correlation potential given by the electron-hole pair (top), the plasmon (middle), and the total (bottom) for $t = -5$ (red) and -50 (black).

matics, so it might be the consequence of using a crude algorithm. Apart from this, it is very similar with Figure 5 and 6. The plasmon is no longer the dominant part. The corresponding V_{xc} is comparable with the one for e-h pair. This is caused by the different behavior of the plasmon in 2D and 3D. In 2D, it has a higher critical momentum since it is mixed with e-h pair asymptotically. As discussed in Sect. 3, the lower the critical momentum is, the stronger the structure of plasmon part.

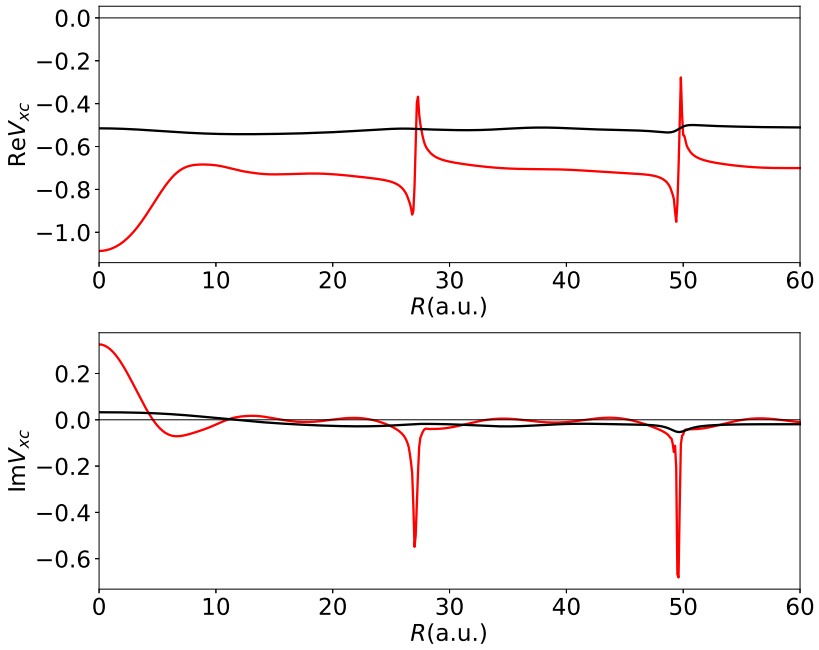

Figure 19: The real and imaginary parts of the exchange-correlation potential for $t = -5$ (red) and -50 (black).

The real and imaginary part of the exchange-correlation potential are shown in Figure 19. The cancellation between exchange and correlation is still revealed clearly despite of the low accuracy of the algorithm. It is most evident for $t = -50$, which is almost a constant. By associating these universal constants with the ground state density, it provides the possibility to develop a LDA as in DFT that is good enough in general.

5 Results for the Hubbard dimer

5.1 Hubbard dimer in the RPA

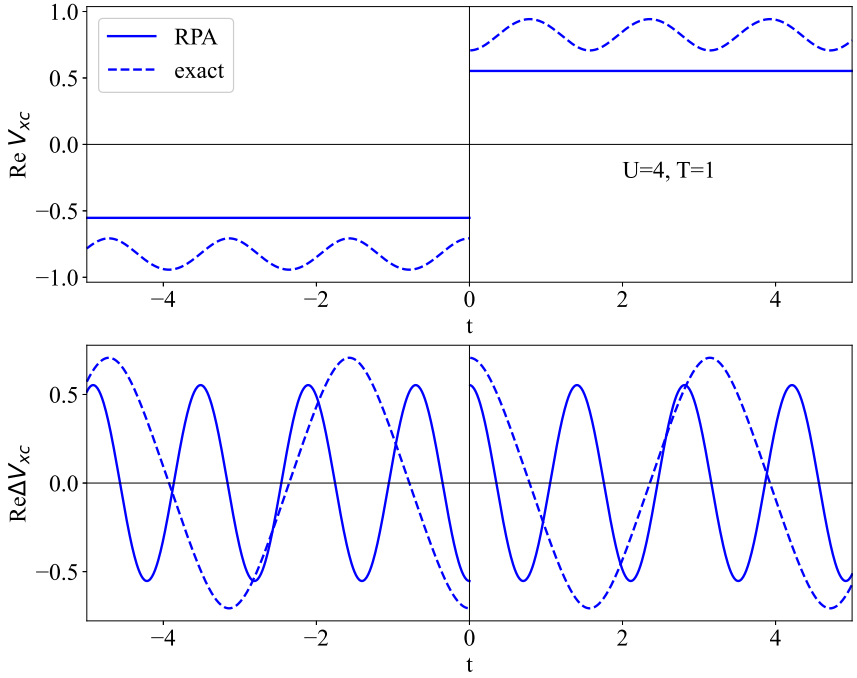

Figure 20: The real part of the exchange-correlation potential for the exact result (dashed blue) and the result given by the RPA (solid blue) for the case $U = 4,\ T = 1$.

As a solvable model, the Hubbard dimer is a good testing ground for gauging the approximations. The analytical results of the exchange-correlation potential of the half-filled Hubbard dimer were presented in [7], and reported here:

$$V^{\mathrm{xc}}(t>0) \equiv V^{\mathrm{xc}}_{AA,AA} = V^{\mathrm{xc}}_{BB,BB} = \frac{\alpha U}{2}\frac{1-\alpha^2 e^{-i4Tt}}{1-\alpha^4 e^{-i4Tt}} \tag{5.1}$$

$$\Delta V^{\mathrm{xc}}(t>0) \equiv V^{\mathrm{xc}}_{AB,BA} = V^{\mathrm{xc}}_{BA,AB} = \frac{\alpha U}{2}\frac{(1-\alpha)^2 e^{-i2Tt}}{1-\alpha^4 e^{-i4Tt}} \tag{5.2}$$

$$V^{\mathrm{xc}}(-t) = -V^{\mathrm{xc}}(t), \quad \Delta V^{\mathrm{xc}}(-t) = -\Delta V^{\mathrm{xc}}(t), \tag{5.3}$$

where Eq. (5.3) is the consequence of the particle-hole symmetry and

$$\alpha = \frac{1-x}{1+x}, \tag{5.4}$$

$$x = \frac{1}{4\Delta}\left(\sqrt{U^2+16\Delta^2} - U\right). \tag{5.5}$$

These results are expressed in the bonding (denoted as B) and antibonding (denoted as A) orbitals that are defined as

$$\varphi_B = \frac{1}{\sqrt{2}}(\varphi_1 + \varphi_2), \varphi_A = \frac{1}{\sqrt{2}}(\varphi_1 - \varphi_2), \tag{5.6}$$

On the other hand, the exchange-correlation potential can also be computed within the RPA. According to the results in Sect. 2.6, results for the dimer can be read

$$t < 0: \quad V^{\mathrm{x}}_{AA,AA} = V^{\mathrm{x}}_{AA,BB} = V^{\mathrm{x}}_{BB,AA} = V^{\mathrm{x}}_{BB,BB} = -\frac{U}{2}, \tag{5.7}$$

$$V^{\mathrm{c}}_{AA,AA} = V^{\mathrm{c}}_{BB,BB} = -\frac{UC}{2}, \quad V^{\mathrm{c}}_{AB,BA} = V^{\mathrm{c}}_{BA,AB} = -\frac{UC}{2}e^{i\Delta t}, \tag{5.8}$$

$$t > 0: \quad V^{\mathrm{x}}_{AA,AA} = V^{\mathrm{x}}_{AA,BB} = V^{\mathrm{x}}_{BB,AA} = V^{\mathrm{x}}_{BB,BB} = -\frac{U}{2}, \tag{5.9}$$

$$V^{\mathrm{c}}_{AA,AA} = V^{\mathrm{c}}_{BB,BB} = \frac{UC}{2}, \quad V^{\mathrm{c}}_{AB,BA} = V^{\mathrm{c}}_{BA,AB} = \frac{UC}{2}e^{-i\Delta t}, \tag{5.10}$$

where

$$C = \frac{\Delta_0 U}{\Delta(\Delta_0 + \Delta)}, \tag{5.11}$$

$$\Delta = \sqrt{\Delta_0^2 + 2U\Delta_0}, \tag{5.12}$$

$$\Delta_0 = \epsilon_A - \epsilon_B. \tag{5.13}$$

In Figure 20, the real part of two components of the exchange-correlation potential for the exact result and the result given by the RPA are shown. The Hubbard dimer is defined with the exchange interaction explicitly removed so that comparison with the the RPA result only applies for the correlation part. It can be seen the anti-symmetry is preserved by both results yielded by exact calculation and the RPA approximation. For the exact result, the particle-hole symmetry has been put in by hand; while for the the RPA result, the time-reversal anti-symmetry exist for the same reason as in electron gas, which is argued in Appendix. A. For the diagonal component V^{xc}, although the time structure of the real part is totally discarded within the RPA, the value is still close to the exact one. For the off-diagonal component, the band gap is overestimated within the RPA compared to the exact one. The underestimation of the intensity for both components of correlation potential is observable.

To see if the RPA can reflect correctly how different U alter the potential, the real part and imaginary part of both orbitals for exact calculation and the RPA are displayed in Figure 21, Figure 22, Figure 23 and Figure 24. It is evident that the intensity of the potential gets incremented with increasing U. Also, the RPA is closer to the exact result when U is smaller as expected.

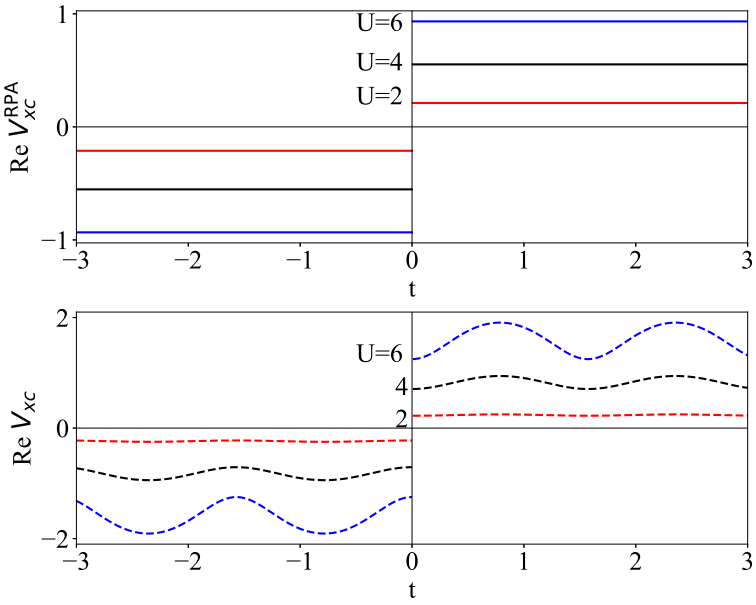

Figure 21: The real part of AA component of the exchange-correlation potential for the exact result (dashed) and the result given by the RPA (solid) for $U = 2$, (red) $U = 4$, (black) $U = 6$ (blue) and $T = 1$.

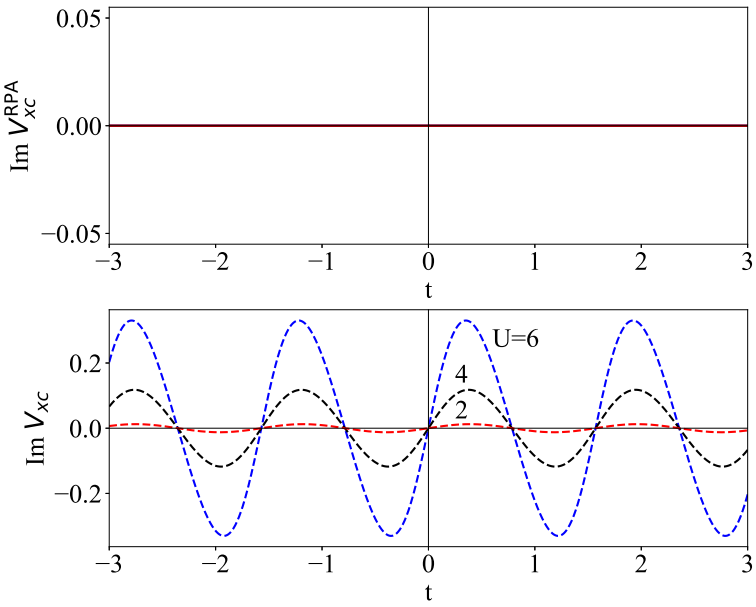

Figure 22: The imaginary part of AA component of the exchange-correlation potential for the exact result (dashed) and the result given by the RPA (solid) for $U = 2$, (red) $U = 4$, (black) $U = 6$ (blue) and $T = 1$.

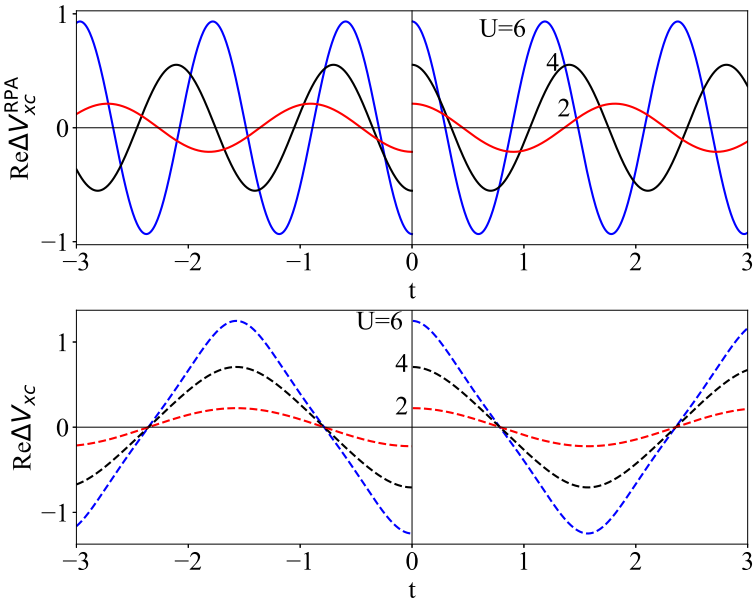

Figure 23: The real part of AB component of the exchange-correlation potential for the exact result (dashed) and the result given by the RPA (solid) for $U = 2$, (red) $U = 4$, (black) $U = 6$ (blue) and $T = 1$.

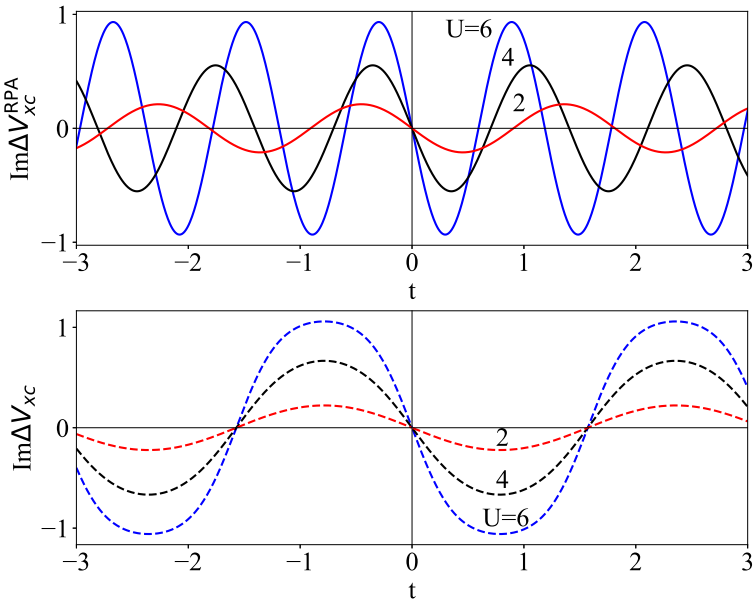

Figure 24: The imaginary part of AB component of the exchange-correlation potential for the exact result (dashed) and the result given by the RPA (solid) for $U = 2$, (red) $U = 4$, (black) $U = 6$ (blue) and $T = 1$.

5.2 Exchange-correlation hole and potential in the RPA with a trial orbital

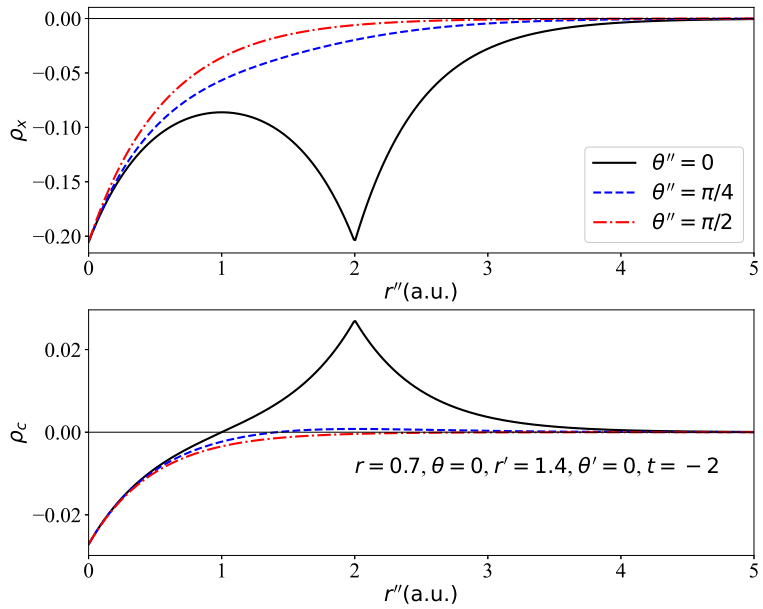

Figure 25: The real part of the exchange and correlation hole for $\theta_2 = 0$ (solid black), $\pi/2$ (dashed blue) and $\pi/4$ (dotted and dashed red) for the case $t = -4.62, r = 0.7, \theta = 0, r' = 1.4, \theta_1 = 0$ in the RPA. .

To explore the fluctuation in the real space, the Hubbard dimer is embedded in a 2D plane due to the angular symmetry. As a crude yet still insightful assumption, the $1s$ orbital of Hydrogen atom is chosen to be the orbital basis of one site in the Hubbard dimer:

$$\psi_{1(2)}(r) = \frac{1}{\sqrt{\pi}} e^{-r}. \tag{5.14}$$

The density fluctuation for three different angles $\theta'' = 0$, $\pi/4$, $\pi/2$ are shown in Figure 25. The relevant parameters are defined in Figure 26. In this figure, one of the sites is put at the origin, while the other is put on the x axis with a specific separation. θ is the polar angle of $\mathbf{r}$, i.e., the angle between positive direction along x axis and $\mathbf{r}$, θ' is the polar angle of $\mathbf{r}'$ and θ'' is the polar angle of $\mathbf{r}''$.

It is apparent that the exchange-only fluctuation shows the similar angular dependence with the one in the 2D HEG. For the correlation hole, this angular dependence is ambiguous for $\theta_2 = \pi/4$ and $\pi/2$. For $\theta_2 = 0$, it can be seen there are two peaks of fluctuations. One is at $r = 0$, and the other is at $r = 2$, where exactly the atoms are just as expected.

In Figure 27, the averaged exchange and correlation hole for $t = \pm 2$ are shown together

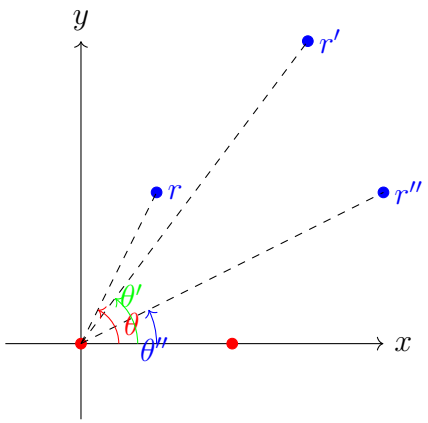

Figure 26: Two sites of the Hubbard dimer (red) and the definition of the variables r, r', r'', θ, θ' and θ''.

in a regular setting of parameters. The anti-symmetry of correlation hole can be easily observed. Also, it is evident that density tend to fulfill the sum rule Eq (2.19), despite it is generated by a trial orbital.

On the one hand, the RPA indicates that the sum rule Eq. (2.19) needs to be fulfilled; on the other hand, half-filling always implies there exists a particle-hole symmetry, which means there should be no difference in any density-related plot for two times with the same magnitude but opposite sign. Therefore, for the exchange part, they are both violated according to 27. Fortunately, it is known that there is no exchange interaction in Hubbard model, i.e., parallel-spin electrons are explicitly prohibited to occupy the same site, and since the RPA correlation hole is assigned with time reversal anti-symmetry, one may still regard the RPA as an option in approximating Hubbard dimer and the generic Hubbard model.

5.3 The spectrum of the Hubbard dimer in the RPA

To investigate how well the RPA does in this case, after plugging the exchange-correlation potential into Eq. (2.8), the Green function is solved and the corresponding spectrum is presented in Figure 28, 29 and 30 respectively.

For $U/T = 0.1$, the spectrum yielded by the RPA is hardly distinguishable from the exact one as it should be because it is the noninteracting Green function used in the RPA, which makes it accurate for weak interaction. For $U/T = 2$, two main peaks in both spectrum are very close as well, but the satellites in the exact spectrum are not reproduced by the RPA, which is as expected since these secondary excitation are just the multiples of the main excitation. For $U/T = 4$, the energy difference between the two main peaks for the RPA becomes less than the exact value, which originates from the use of the

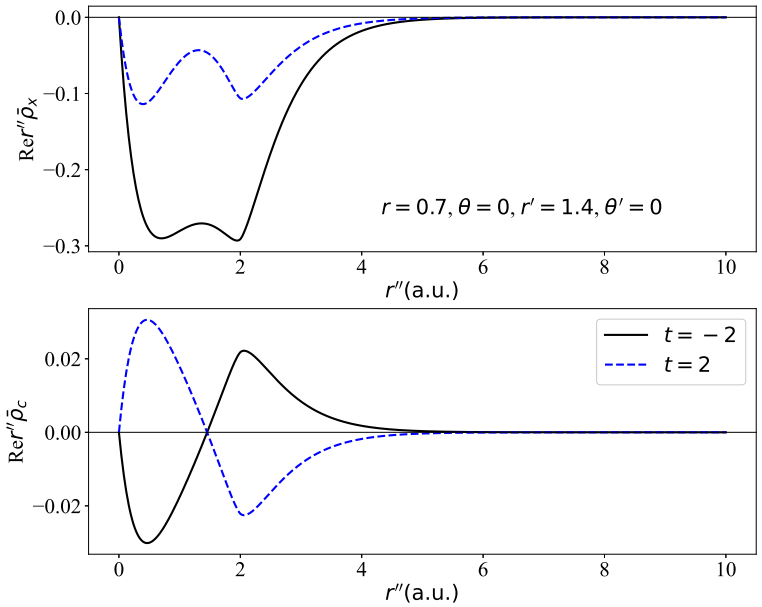

Figure 27: The real part of the exchange and correlation potential for $t = \pm 2$ for the case $r = 0.7, \theta = 0, r' = 1.4, \theta' = 0$ in the RPA. .

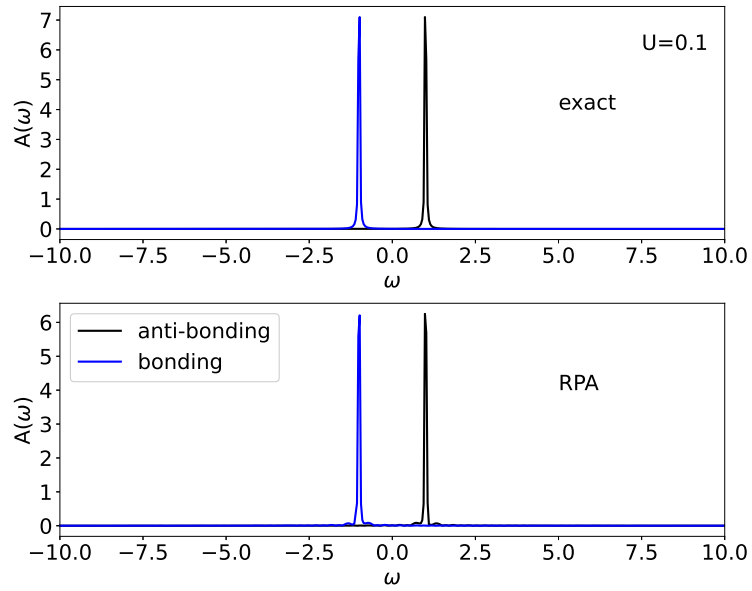

Figure 28: The spectrum yielded by the RPA and the exact one for $U = 0.1$ and $T = 1$, where the contribution of bonding (blue) and anti-bonding (black) are displayed separately. A broadening of 0.01 has been used.

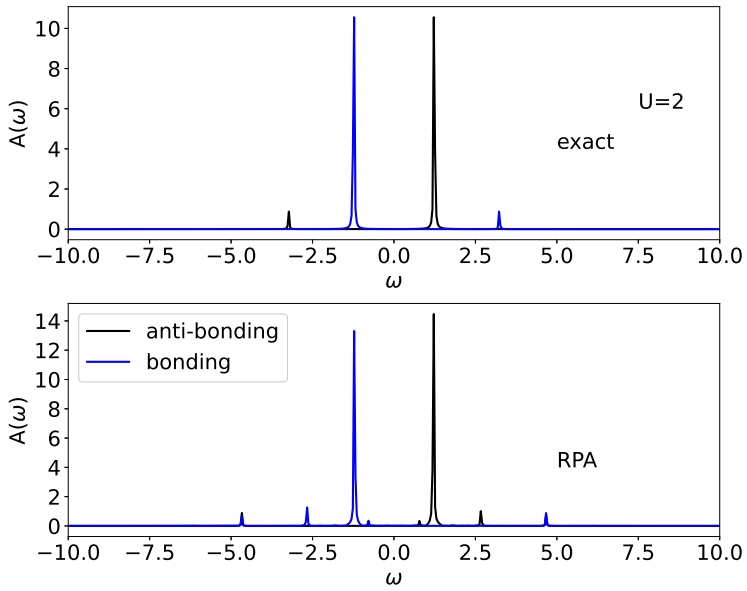

Figure 29: The spectrum yielded by the RPA and the exact one for $U = 2$ and $T = 1$, where the contribution of bonding (blue) and anti-bonding (black) are displayed separately. A broadening of 0.01 has been used.

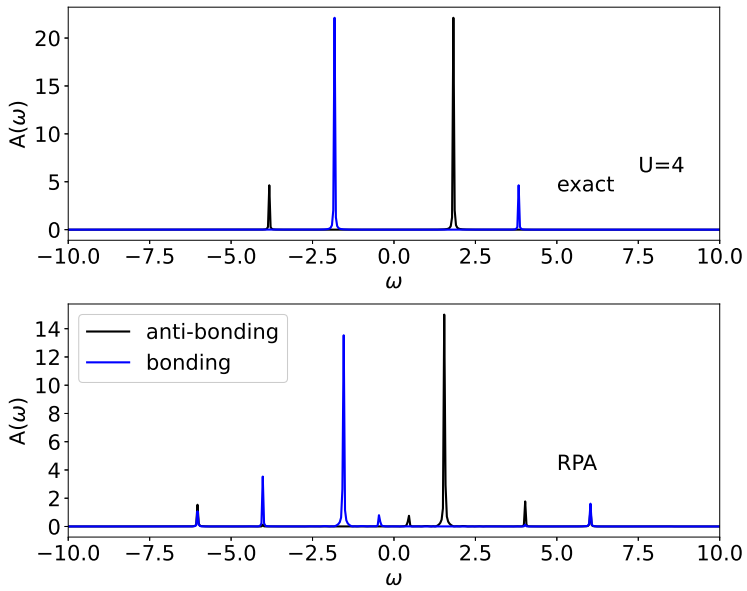

Figure 30: The spectrum yielded by the RPA and the exact one for $U = 4$ and $T = 1$, where the contribution of bonding (blue) and anti-bonding (black) are displayed separately. A broadening of 0.01 has been used.

noninteracting Green function. Note that the excitation in the band gap cannot be given by the exchange correlation potential within the RPA, so it should be the deficiency of the Fourier transforming algorithm.

Although the the RPA cannot give the correct position of main excitations when U/T is large enough, widening of the band gap can be undoubtedly observed. Since the RPA can be easily performed for relatively large systems in arbitrary dimension, it is a good approximation at least to get a sufficiently accurate band gap.

6 Outlook

In Sect. 2, we begun with the presentation of the general formula for the exchange-correlation hole. We then introduced the random-phase approximation (RPA) as a central method within the exchange-correlation formalism, followed by its application to both the three-dimensional (3D) and 2D homogeneous electron gas (HEG). For the dD Hubbard cubic lattice, we derived the relevant formulas and provided concrete expressions used in computations, aiding future research on specific Hubbard models.

While the formalism for the 3D HEG has been established for some time, the complexity of the linear density response function and the high dimensionality of the integrals present challenges in computing the correlation hole and potential accurately. Consequently, we exclusively presented the correlation potential in Sect. 3. Due to the computational limitation concerning expressions of the form $0/0$, contributions from electron-hole pairs and plasmons were considered separately. Notably, the dominance of the plasmon contribution explains the agreement between results obtained using the plasmon-pole approximation and exact computations, especially regarding the cancellation between exchange and correlation.

For the 2D HEG, we presented results in parallel with those for the 3D HEG [6], compensating for the reduction in dimensionality with an increase in density fluctuation scale. By exploring angular and temporal dependencies, we demonstrated the significance of holes rather than electrons at least for exchange interaction in the electron gas. Additionally, we presented and compared the spherical-averaged exchange density with the Hartree-Fock approximation (HFA), showing strong structure for intermediate radial separation R. The time and radial separation dependence of deviation from HFA are investigated separately, revealing deviations that grow with time, yet remain close to zero except for a series of peaks whose height monotonically decreases. The corresponding dependencies are investigated in the 3D case as well, which exhibit quite different behavior. This can find explanation in mathematics yet the physics meaning still needs to be investigated.

In the Hubbard dimer, where exchange is explicitly eliminated, only correlation effects are used for comparison with exact results. We found that the potential closely approximates the exact one when the interaction parameter U/t is small, as expected. However, details introduced by stronger interactions are lost in this approximation. Nevertheless, the sum rule is satisfactorily fulfilled even with a simple trial function. Furthermore, the spectrum obtained by solving the equation of motion of the Green function in the RPA exhibits significant quantitative resemblance to the exact spectrum for the main peaks. Additionally, the accidental preservation of time-reversal anti-symmetry by the RPA suggests its potential in approximating the generic Hubbard model, particularly in determining band gaps.

This work marks the first full RPA calculation. The cancellation between exchange and correlation, leading to a nearly constant potential when time is large, validates a simple ansatz for exchange-correlation potential that is introduced in [7, 8]. In this ansatz,

the exchange-correlation potential has only two terms: one is a constant and the other is exponential in terms of the frequency of collective modes in the system. Despite its simplicity, it can reproduce the benchmark results surprisingly well [11, 12]. Additionally, the application of the RPA in the Hubbard dimer demonstrates its reliability, where the exchange-correlation potential is also in this simple form. All of these facts provide us the possibility to develop a RPA-based LDA based on this ansatz. The further effort will be spent on exploring the range of application and how it should be parameterized.

The results for the Hubbard model in any dimension will be very useful in calculating the exchange-correlation potential in specific finite lattices. Furthermore, the results such as the spectrum and the total energy need to be compared with the bench mark results in order to evaluate its quality. The dimension of the model and the size of the lattice need to be varied carefully to explore the range of application.

This work also lays the groundwork for future researchs on the 2D electron gas. While some important and unique features of the 2D electron gas, particularly those related to superconductivity and magnetism, are not yet incorporated into the exchange-correlation formalism, addressing these aspects would enrich the picture provided by the formalism, offering straightforward and insightful interpretations.

References

[1] B. Holm and F. Aryasetiawan, Phys. Rev. B **62**, 8 (2000).

[2] F. Aryasetiawan, Phys. Rev. B **105**, 075106 (2022).

[3] J. C. Slater, Phys. Rev. **81**, 385 (1951).

[4] P. Hohenberg and W. Kohn, Phys. Rev. **136**, B864 (1964).

[5] W. Kohn and L. J. Sham, Phys. Rev. **140**, A1133 (1965).

[6] K. Karlsson and F. Aryasetiawan, Phys. Rev. B **107**, 115172 (2023).

[7] F. Aryasetiawan and T. Sjöstrand, Phys. Rev. B **106**, 045123 (2022).

[8] Z. Zhao, C. Verdozzi, and F. Aryasetiawan, Phys. Rev. B **108**, 235132 (2023).

[9] B. Mihaila, arXiv:1111.5337.

[10] A. L. Fetter and J. D. Walecka, *Quantum Theory of Many-particle Systems* (Dover, Mineoal, NY, 2003).

[11] L. Hedin, Phys. Rev. **139**, A796 (1965).

[12] F. Aryasetiawan and O. Gunnarsson, Rep. Prog. Phys. **61**, 237 (1998).

Acknowledgements

The author is very grateful for the great help from the supervisor Ferdi. Aryasetiawan. The exchange-correlation formalism cannot be established so well without his wisdom and effort. His profound knowledge and experience in the field of DFT captures a valuable usage of this formalism, namely developing a LDA based on it. Personally, without his patient tutoring and important advice during this year, it is impossible for this thesis can be completed even in such a hasty way.

Because of the time constraint, there have been no satisfactory results for correlation potential in 3D so far until Krister. Karlsson provided his output by careful computation. His patience in every discussion on the computation details is greatly appreciated.

The author also would like to thank the technical help involves the details of codes from the co. supervisor Zhen. Zhao.

A Correlation potential of dD Hubbard cubic lattice in the RPA

Within the RPA, the response function is given by

$$\chi(r,r';\omega) = P^0(r,r';\omega) + \int d^3r_1 d^3r_2 P^0(r,r_1;\omega) v(r_1-r_2)\chi(r_2,r';\omega), \tag{A.1}$$

To make life easier, assume $\varphi_{\mathbf{k}}$s are real and ω is not equal to any of the poles so that one does not need to worry about the weight of imaginary part.The polarization has been given by Eq. (2.21), which can be written as

$$P^0(r,r';\omega) = \sum_{\mathbf{k}_i}^{\text{occ}} \sum_{\mathbf{k}_h}^{\text{unocc}} \varphi_{\mathbf{k}_i}(r)\varphi_{\mathbf{k}_h}(r)\varphi_{\mathbf{k}_i}(r')\varphi_{\mathbf{k}_h}(r') \left\{ \frac{2}{\omega - \Delta^0_{hi} + i\delta} - \frac{2}{\omega + \Delta^0_{hi} - i\delta} \right\}, \tag{A.2}$$

where $\Delta^0_{ih} = \varepsilon_{\mathbf{k}_h} - \varepsilon_{\mathbf{k}_i}$. It is clear that $\chi(r,r';\omega)$ has the same form,

$$\chi(r,r';\omega) = \sum_{\mathbf{k}_i}^{\text{occ}} \sum_{\mathbf{k}_h}^{\text{unocc}} \varphi_{\mathbf{k}_i}(r)\varphi_{\mathbf{k}_h}(r)\varphi_{\mathbf{k}_i}(r')\varphi_{\mathbf{k}_h}(r') \left(\frac{\alpha_{hi}}{\omega - \Delta_{hi} + i\delta} - \frac{\alpha_{hi}}{\omega + \Delta_{hi} - i\delta} \right), \tag{A.3}$$

whereΔ_{hi} and α_{hi} are to be determined. Plug it into Eq. (A.1), then one get

$$\chi_{ih}(\omega) = P^0_{ih}(\omega) + \frac{U}{N} \sum_{\mathbf{k}_l} \sum_{\mathbf{k}_j} \delta_{\mathbf{k}_l+\mathbf{k}_h} \delta_{\mathbf{k}_j+\mathbf{k}_i} P^0_{lj}(\omega)\chi^0_{ih}(\omega). \tag{A.4}$$

Due to the orthogonality of orbitals, it yields

$$\Delta_{hi} = \sqrt{(\Delta^0_{hi})^2 + \frac{4U}{N}\Delta^0_{hi}}, \qquad \alpha_{hi} = \frac{2\Delta^0_{hi}}{\Delta_{hi}}. \tag{A.5}$$

So the response function in time domain is given by

$$\chi(r,r';\omega)=\sum_{\mathbf{k}_i}^{\text{occ}}\sum_{\mathbf{k}_h}^{\text{unocc}}\varphi_{\mathbf{k}_i}(r)\varphi_{\mathbf{k}_h}(r)\varphi_{\mathbf{k}_i}(r')\varphi_{\mathbf{k}_h}(r')(-i\alpha_{hi})\left\{\theta(t)e^{-i\Delta_{hi}t}+\theta(-t)e^{i\Delta_{hi}t}\right\}. \tag{A.6}$$

Then according to Eq(2.7), the correlation term is given by

$$\begin{aligned}
&\rho_{\text{c}}(r,r',r'';t)G^0(r,r';t)=i\int dr_4dt_4\Big\{i\theta(t_4-t)\\
&\sum_{\mathbf{q}}^{\text{occ}}\varphi_{\mathbf{q}}(r)\varphi_{\mathbf{q}}(r_4)e^{-i\epsilon_{\text{q}}(t-t_4)}-i\theta(t-t_4)\sum_{\mathbf{q}'}^{\text{unocc}}\varphi_{\text{q}'}(r)\varphi_{\text{q}'}(r_4)e^{-i\epsilon_{\text{q}'}(t-t_4)}\Big\}\\
&\times\int dr_5v(r_4-r_5)\sum_{\mathbf{k}_j}^{\text{occ}}\sum_{\mathbf{k}_l}^{\text{unocc}}\varphi_{\text{k}_j}(r_5)\varphi_{\text{k}_l}(r_5)\varphi_{\text{k}_j}(r'')\varphi_{\text{k}_l}(r'')(-i\alpha_{lj})\\
&\left\{\theta(t_4-t)e^{-i\Delta_{lj}(t_4-t)}+\theta(t-t_4)e^{i\Delta_{lj}(t_4-t)}\right\}\times\Big\{i\theta(-t_4)\sum_{\mathbf{p}}^{\text{occ}}\varphi_{\text{p}}(r_4)\varphi_{\text{p}}(r')e^{-i\varepsilon_{\text{p}}t_4}\\
&-i\theta(t_4)\sum_{\mathbf{p}'}^{\text{unocc}}\varphi_{\text{p}'}(r_4)\varphi_{\text{p}'}(r')e^{-i\varepsilon_{\text{p}'}t_4}\Big\}.
\end{aligned}\tag{A.7}$$

For $t<0$, after substituting the Fourier expansion of each bloch orbital and making use of the local property of the interaction, i.e.

$$U=\int d^3rd^3r'\varphi_i(r)\varphi_i(r)v(r-r')\varphi_i(r')\varphi_i(r'), \tag{A.8}$$

it becomes

$$\begin{aligned}
&\rho_{\text{c}}(r,r',r'';t)G^0(r,r';t)\\
=&(i)^3\sum_{\mathbf{k}_j}^{\text{occ}}\sum_{\mathbf{k}_l}^{\text{unocc}}\sum_{\mathbf{q}}^{\text{occ}}\sum_{\mathbf{p}'}^{\text{unocc}}\frac{U}{N}\delta_{\mathbf{p}'+\mathbf{k}_l,\mathbf{q}+\mathbf{k}_j+(2\pi)/a\hat{\mathbf{v}}}\alpha_{lj}\frac{-e^{-i(\varepsilon_{\mathbf{q}}-\Delta_{lj})t}}{\varepsilon_{\mathbf{q}}-\Delta_{lj}-\varepsilon_{\mathbf{p}'}}\varphi_{\text{q}}(r)\varphi_{\text{p}'}(r')\varphi_{\text{k}_j}(r'')\varphi_{\text{k}_l}(r'')\\
&+(i)^3\sum_{\mathbf{q}'}^{\text{unocc}}\sum_{\mathbf{k}_j}^{\text{occ}}\sum_{\mathbf{k}_l}^{\text{unocc}}\sum_{\mathbf{p}}^{\text{occ}}\frac{U}{N}\delta_{\mathbf{k}_l+\mathbf{p},\mathbf{q}'+\mathbf{k}_j}\alpha_{lj}\frac{e^{-i\varepsilon_{\mathbf{k}_j}t}}{\varepsilon_{\mathbf{q}'}+\Delta_{lj}-\varepsilon_{\mathbf{p}}}\varphi_{\text{q}'}(r)\varphi_{\text{p}}(r')\varphi_{\text{k}_j}(r'')\varphi_{\text{k}_l}(r'')
\end{aligned}\tag{A.9}$$

So, the matrix element $(V_{\text{c}}G^0)_{mn}$ is

$$\begin{aligned}
\sum_{\mathbf{k}_u}^{\text{occ}}V_{\text{c}}^{mu,un}G_u^0=&-i\sum_{\mathbf{k}_j}^{\text{occ}}\sum_{\mathbf{k}_l}^{\text{unocc}}\alpha_{lj}\left(\frac{U}{N}\right)^2\\
&\Big\{\sum_{\mathbf{q}}^{\text{occ}}\sum_{\mathbf{p}'}^{\text{unocc}}\delta_{\mathbf{p}'+\mathbf{k}_l,\mathbf{q}+\mathbf{k}_j+(2\pi)/a\mathbf{v}}\delta_{\mathbf{q}+\mathbf{k}_j+(2\pi)/a\mathbf{v},\mathbf{k}_m+\mathbf{k}_l}\delta_{\mathbf{p}',\mathbf{k}_n}\frac{-e^{-i(\varepsilon_{\mathbf{q}}-\Delta_{lj})t}}{\varepsilon_{\mathbf{q}}-\Delta_{lj}-\varepsilon_{\mathbf{p}'}}\\
&+\sum_{\mathbf{q}'}^{\text{unocc}}\sum_{\mathbf{p}}^{\text{occ}}\delta_{\mathbf{k}_l+\mathbf{p},\mathbf{q}'+\mathbf{k}_j}\delta_{\mathbf{q}'+\mathbf{k}_j,\mathbf{k}_m+\mathbf{k}_l+(2\pi)/a\mathbf{v}}\delta_{\mathbf{p},\mathbf{n}}\frac{e^{-i\varepsilon_{\mathbf{k}_j}t}}{\varepsilon_{\mathbf{q}'}+\Delta_{lj}-\varepsilon_{\mathbf{p}}}\Big\}.
\end{aligned}\tag{A.10}$$

Those three Kronecker Delta cancels only two summation, which yields

$$\sum_{\mathbf{k}_i} V_{\mathrm{c}}^{mi,im} e^{-i\varepsilon_{\mathbf{k}_i} t} = \sum_{\mathbf{k}_j}^{\mathrm{occ}} \sum_{\mathbf{k}_l}^{\mathrm{unocc}} \alpha_{jl} \frac{U^2}{N^2} \begin{cases} -\frac{e^{-i(\varepsilon_{\mathbf{q}} - \Delta_{lj})t}}{\varepsilon_{\mathbf{q}} - \Delta_{lj} - \varepsilon_{\mathbf{k}_m}}, & \mathbf{k}_m \in \mathrm{unocc} \\ \frac{e^{-i\varepsilon_{\mathbf{k}_m} t}}{\varepsilon_{\mathbf{q}'} + \Delta_{lj} - \varepsilon_{\mathbf{k}_m}}, & \mathbf{k}_m \in \mathrm{occ} \end{cases} \tag{A.11}$$

where

$$\mathbf{q} = \mathbf{k}_m + \mathbf{k}_l - \mathbf{k}_j - \frac{2\pi}{a}\hat{\mathbf{v}}, \quad \mathbf{q}' = \mathbf{k}_m + \mathbf{k}_l - \mathbf{k}_j \tag{A.12}$$

and

$$\hat{\mathbf{v}} = a \sum_{i=1}^{d} \hat{\mathbf{x}}_i. \tag{A.13}$$

Similarly, for $t > 0$, the correlation potential is given by

$$\sum_{\mathbf{k}_i} V_{\mathrm{c}}^{mi,im} e^{-i\varepsilon_{\mathbf{k}_i} t} = -\sum_{\mathbf{k}_j}^{\mathrm{occ}} \sum_{\mathbf{k}_l}^{\mathrm{unocc}} \alpha_{jl} \frac{U^2}{N^2} \begin{cases} \frac{e^{-i(\varepsilon_{\mathbf{q}'} + \Delta_{lj})t}}{\varepsilon_{\mathbf{p}'} + \Delta_{lj} - \varepsilon_{\mathbf{k}_m}}, & \mathbf{k}_m \in \mathrm{occ} \\ -\frac{e^{-i\varepsilon_{\mathbf{k}_m} t}}{\varepsilon_{\mathbf{q}} - \Delta_{lj} - \varepsilon_{\mathbf{k}_m}}, & \mathbf{k}_m \in \mathrm{unocc} \end{cases} \tag{A.14}$$